Reduced RNA turnover as a driver of cellular senescence

Nowsheen Mullani, Mickaël Costallat, Eric Batsche, Yevheniia Porozan, Ida C Guerrera, Michele Goodhardt, Giovanni Cenci, Christian Muchardt

Reduced RNA turnover as a driver of cellular senescence

Nowsheen Mullani[1,2], Mickaël Costallat[1], Eric Batsché[1], Yevheniia Porozan[1], Ida C. Guerrera[3], Michele Goodhardt[4], Giovanni Cenci[5], Christian Muchardt[1]

(1) Institut Pasteur, CNRS UMR3738, Dpt Biologie du Développement et Cellules Souches, Unité de Régulation Epigénétique, Paris, France.
(2) Sorbonne Université, Ecole Doctorale "Complexité du Vivant" (ED515), F-75005 Paris, France
(3) Proteomics Platform 3P5-Necker, Université Paris Descartes - Structure Fédérative de Recherche Necker, INSERM US24/CNRS UMS3633, Paris, France.
(4) INSERM UMRS-1126, Institut Universitaire d'Hématologie, Université Paris Diderot, Paris, France.
(5) Istituto Pasteur Italia - Fondazione Cenci Bolognetti, Rome, Italy.

ABSTRACT

Accumulation of senescent cells is an important contributor to chronic inflammation upon aging. While cytoplasmic DNA was shown to drive the inflammatory phenotype of senescent cells, an equivalent role for RNA has never been explored. Here, we show that cellular senescence correlates with reduced expression of RNA exosome subunits and coincident accumulation of promoter RNAs and immature RNA transcripts. Forced accumulation of these RNAs by inactivation of the Exosc3 exosome subunit induces expression of senescence markers and reduced mitochondrial gene expression. Reciprocally, mitochondrial suffering and oxidative stress results in reduced RNA decay, suggestive of a feedback loop between RNA decay and mitochondrial activity. As several of the accumulating RNAs are also produced during normal activation of immune cells and contain Alu sequences known to trigger an innate immune response, we propose that stabilizing immature and unstable RNAs participate in driving and maintaining the permanent inflammatory state characteristic of cellular senescence.

INTRODUCTION

Cellular senescence is a state of irreversible cell cycle arrest (1). Experimentally, it can be triggered via multiple routes including prolonged maintenance in tissue culture, exposure to ionizing radiations, force expression of mitogenic oncogenes, or exposure to oxidative stress. These inducers of senescence all share the ability to cause DNA damage and to generate reactive oxygen species, two components that probably are at the basis of the phenomenon (2). One of the hallmarks of senescent cells is their production of a range of chemokines, proinflammatory cytokines, growth factors, and matrix-remodelling enzymes, defining the senescence-associated secretory phenotype or SASP. This proinflammatory characteristic has a crucial role in propagating senescence and in recruiting immune cells to the senescent tissue. As senescent cells accumulate with time, SASP is also believed to be a major determinant of the chronic low-grade inflammation associate with age and age-related diseases.

SASP activation is largely orchestrated by nuclear factor (NF)-kB and CCAAT/enhancer-binding protein beta (C/EBPb). Upstream of these transcription factors, DNA damage and the DNA damage response (DDR) are majors triggers of the proinflammatory pathways (3). Yet, it seems that other mechanisms may allow nucleic acids to drive the chronic sterile inflammation characteristic of cellular senescence. Indeed, several studies have associated senescence with an accumulation of DNA in the cytoplasm. This DNA, in the form of chromatin, triggers innate immunity via the cytosolic DNA-sensing cGAS–STING pathway (4). Cytoplasmic DNA possibly originates from chromosome segregation errors during mitosis and its accumulation seems favoured by down-regulation in senescent cells of cytoplasmic DNases (5). As an alternative or a complement, it has further been shown that in senescent cells, de-repression of repeat elements of the LINE family results in the production of retroviral RNAs, that after retrotranscription, accumulate in the cytoplasm in the form of cDNAs (6).

Consistent with a role of cytoplasmic DNA, multiple studies have documented the importance of the interferon pathway in driving senescence, and suppression of type 1 interferon signalling hinders onset of senescence (7). The interferon pathway was initially described as an antiviral defence mechanism activated upon detection by specific cytoplasmic or endosomal receptors of either viral DNA or double stranded RNA. In that context, RNA could also be a trigger of senescence. Yet, the role of RNA in senescence has mostly been examined in the nuclear compartment, where specific long non-coding RNAs (lncRNAs) participate in the regulation of genes relevant for cellular senescence (8,9) (10). Some observations are suggestive of a more comprehensive impact of RNAs in cellular senescence, via their production, their maturation, or their turn-over. For example, it was reported that in the aging mouse brain, some neurons start accumulating 3′ untranslated regions (UTRs), resulting in the production of small peptides of yet unknown function (11). In parallel, transcripts from SINEs/Alus, a family of repetitive elements particularly abundant in euchromatin, have been reported to accumulate in senescent cells with an impact on genome integrity (12). Finally, several studies have reported that cellular senescence is associated with numerous changes in the outcome of alternative pre-mRNA splicing (13). This results in the production of senescent toxins including progerin, a variant of Lamin A associated with the Hutchinson-Gilford progeria syndrome (14), while also favoring the synthesis of S-Endoglin and p53beta that may have a similar pro-senescence activity (15) (16).

Whether RNAs have an effect on cellular senescence independently of their ability to regulate specific genes in the nucleus or to encode proteins has never been specifically investigated. Here, we examined senescent cells of different origins for sources of RNA species liable to activate innate immunity pathways. This approach revealed that senescence is associated with a gradual accumulation of alternative splicing products, but also of several lncRNAs, including many upstream antisense RNAs (uaRNAs) and improperly maturated U snRNAs. This seemingly heterogeneous population of RNAs shared however a decay process dependent on the RNA exosome (17) and further examination of the transcriptomes revealed that all the various senescent cells under scrutiny displayed strongly reduced expression of at least one component of the RNA decay machinery. Consistent with a pro-senescence activity of the accumulating RNAs, we further show that inactivation of RNA exosome activity in mouse cells gives rise to a senescent phenotype. Interestingly, the decreased RNA exosome activity also resulted in reduced transcription of many mitochondrial genes, while, inversely, mitochondrial dysfunction lead to reduced expression of key component of the RNA exosome and accumulation of heterogeneous RNA species. This suggested that the RNA exosome and the mitochondria are linked in a feedback loop driven by reactive oxygen species (ROS) and possibly involved in the permanent inflammatory state of senescent cells. Finally, examination of the lncRNAs accumulating in senescent cells revealed that they frequently contain SINE/Alu sequences as a consequence of transcription reaching beyond an SINE/Alu-free regions surrounding most promoters. As production of SINE/Alu-containing RNAs is frequent in immune cells and readily detected in activated T and B cells, we propose that these RNAs function as adjuvant to the inflammatory reaction during normal cellular defence, while also having the potential of driving chronic inflammation for the onset and the maintenance of cellular senescence.

RESULTS

Reduced RNA turnover in senescent cells

To gain a global insight in mRNA maturation and turnover in senescent cells, we reanalyzed publicly available RNA-seq data from IMR90 cells driven into senescence by expression of oncogenic RAS for 0, 4, or 10 days (18). The multiple time points and the availability of 4 replicates for each time point made this data suitable for global analysis of splicing products. This analysis uncovered a progressive accumulation of splice variants while the cells were driven toward senescence (Figure 1A). Unexpectedly, these splice variants were of any possible kind (increased inclusion, increased exclusion, alternative C-terminus *etc*…), more suggestive of reduced quality control, than of regulated RNA splicing. As mis-spliced mRNA species are normally subject to degradation by the RNA exosome (17), we examined expression of the core subunits of this RNA surveillance machinery. This revealed that the catalytic subunit DIS3L as well as the auxiliary subunits EXOSC2, EXOSC3, EXOSC6, EXOSC8, EXOSC9, EXOSC10, and HBS1L were progressively downregulated as the cells entered senescence (Figure 1B). Two subunits, namely EXOSC4 and EXOSC5, that both are paralogs of EXOSC6, were upregulated during this time, possibly to compensate for the decreased availability of EXOSC6.

To determine whether increased accumulation of splice variants was observed in other senescent cells, we analyzed a second set of data from either fibroblasts, keratinocytes, or melanocytes driven into senescence by ionizing radiation (19). RNA from these cells was sequenced at days 0, 4, 10, and 20. In fibroblasts and keratinocytes, splice variants gradually accumulated during the 20 days. Both cell lines

recapitulated a downregulation of multiple subunits of the RNA exosome, with strongest effects on EXOSC2, EXOSC8, and EXOSC9 (Sup Figure 1A-1D). In the melanocytes, we observe a strongly increased accumulation of splice variants between days 0 and 4 or 10, and then a decrease at day 20. Possibly, at the late time points, the cell population may have been overgrown by cells not having entered senescence, a possibility that is consistent with the re-expression of genes related to S-phase and cell-cycle described in the initial paper (19). The melanocytes also singled out by a moderate up- rather than down-regulation of several core RNA exosome subunits. Instead, we detected down-regulation of PABPC1, PABPC3, and EIF3E, involved in cytoplasmic turnover of polyadenylated mRNAs (Sup Figure 1E-1F).

The reduced quality control of mRNA splicing products prompted us to search senescent cells for other indications of reduced RNA turnover. For that, we identified a set of RNA-seq data from either proliferating or senescent Wi38 cells having a sequencing depth sufficient for the detection of rare RNAs (20). In these cells, it was DIS3L, the catalytic subunit of the cytoplasmic RNA exosome that was down-regulated (Sup Figure 1G). To identify effects of reduced RNA turnover, we compared this data set to one from HeLa cells depleted of EXOSC3 by siRNAs (21). We first examine histone genes because of their high expression levels allowing easy detection of non-maturated mRNAs. In the senescent cells, histone gene expression was overall decreased as a likely consequence of the growth-arrested. Yet, reads were accumulating downstream of these genes, in a manner very similar to that observed upon depletion of EXOSC3 (see examples of HIST2H4B Figure 1C and Sup. 1H, and HIST1H3D and HIST1H2BF Sup. Figure 1I). Observation of the histone genes also revealed accumulation of upstream antisense RNAs (uaRNAs) at promoters. These RNAs are produced as a consequence of the divergent transcription occurring at sites of transcription initiation (schematic Figure 1D). These RNAs are normally degraded rapidly by the RNA exosome. Accumulation of uaRNAs was also observed at many less expressed genes (see example of the H6PD gene Figure 1E and 119 additional examples in Sup. Table 1A). In all the cases where the genes were also expressed in HeLa cells, a similar accumulation of uaRNAs was observed upon inactivation of EXOSC3 (Figure 1F). Quantification at the series of 5260 promoters not overlapping with coding regions of any gene revealed an average increase in accumulation of uaRNA in the senescent cells of approximately 10% (Fig 1G and 1H).

In addition to the uaRNAs, we further observed accumulation of immature U snRNAs in the senescent Wi38 cells, an accumulation that again was matching the effect of EXOSC3 depletion in HeLa cells (Figure 1I). This effect was seen essentially at all U snRNA genes expressed in the Wi38 cells (Figure 1J). Finally, we noted an interesting accumulation of the 3'UTR region of histone gene HIST2H2BE in both senescent and EXOSC3-depleted cells (Figure 1K). This phenomenon was reminiscent of the accumulation of 3'UTRs previously described in the aging mouse brain (11).

Altogether, these data show an accumulation in senescent cells of several RNA species as a consequence of the systematic impairment of the RNA decay machinery in these cells. Hereafter, for shortness, we will refer to accumulating RNAs downstream of genes, uaRNAs, and immature U snRNAs as "senescence-signature RNAs".

Senescent cells share an RNA signature with cells exposed to H2O2

Accumulation of uaRNAs has previously been observed in cells exposed to oxidative stress, a central determinant of senescence ((22,23) and example of the H6PD gene in Figure 2A). This phenomenon referred to as "creeping RNAPII" was imputed to

defective RNA polymerase II transcription termination (23). To investigate a possible continuity between oxidative stress and senescence at the level of the RNA accumulating in the cells, we examined cells exposed to H2O2 for the presence of senescence-signature RNAs other than uaRNAs. For this study, we chose a data set from H2O2-treated BJ or MRC5 cells allowing for detection of rare RNAs (22). In this data, we observed a so far overseen accumulation of reads downstream of many histone genes, alike what we had observed in the senescent Wi38 cells and in HeLa cells depleted of EXOSC3 (Figures 2B). We also observed an accumulation of immature U snRNAs (see example in Figure 2C and heatmap of Figure 2D). Finally, we noted the stabilization of the long 3' UTR of HIST2H2BE in all the cell lines (Figures 2E). These observations indicate that the "senescence-signature RNAs" defined in Figure 1 are also accumulating in cells exposed to H2O2. When examining the RNA degradation machinery in these cells, we observe in both BJ and MRC5 cells, a decreased expression of several RNA exosome core subunits and of the Ski2-like cytoplasmic helicase SKIV2L, particularly visible at the longer time point. Together, these data suggest that, in cells exposed to H2O2, the accumulation of uaRNAs may be the combined effect of increased production and length of these RNAs by the "creeping RNAPII" and the stabilization of the same as a result of reduced RNA decay. We further speculate that the very rapid effect of H2O2 on RNA accumulation may also involve a possible inactivation of the RNA exosome activity by damaging oxidation or phosphorylation by stress-related kinases (24).

Prolonged RNA exosome depletion induces a senescent phenotype.

With the objective of identifying a possible function for senescence-signature RNAs, we next explored the long-term effect of conditions promoting their accumulation. To that end, we examined a dataset from mouse embryonic stem cells depleted from Exosc3 for 3 days (25). As expected and described in the original paper, these cells recapitulated the increased accumulation uaRNAs (example in Figure 3A). They also recapitulated the effect on U snRNA maturation (example in Figure 3B). Interestingly, GO term analysis of genes up-regulated upon this long-term Exosc3 inactivation revealed a highly significant enrichment in genes associated with the p53 pathway and we pinpointed an increased expression of both Cdkn1a (p21) and Cdkn2a (p16), two markers of cellular senescence (Figure 3C and 3D, and Sup. Table 3 listing differentially regulated genes associated with the GO terms). Consistent with this, downregulated genes were highly enriched in genes associated with cell cycling (Figure 3E). From these observations, we concluded that loss of RNA exosome activity results in a transcriptional landscape characteristic of senescent cells.

Examining GO terms for cellular compartments further highlighted a significant enrichment in mitochondrial genes among the genes down-regulated by depletion of ExoSC3 (Figure 3F). This was consistent with an earlier report showing mitochondrial suffering in patients with pontocerebellar hypoplasia, a syndrome linked to a mutation in the ExoSC3 gene (26). This observation prompted us to examine a mouse model associated with mitochondrial suffering. Based on RNA-seq data quality, we chose to examine mice inactivated for Mof, a histone acetylase regulating transcription and respiration in mitochondria (27). Inactivation of this gene has catastrophic consequences on tissues with high-energy consumption, triggering hypertrophic cardiomyopathy and cardiac failure in murine hearts. At a cellular level,

cardiomyocytes show severe mitochondrial degeneration and deregulation of mitochondrial nutrient metabolism and oxidative phosphorylation pathways. Consistent with mitochondrial suffering and ensuing oxidative stress, Mof inactivation reproduced the increased accumulation uaRNAs. To illustrate this, Figure 3A shows the example of the Klf6 gene, while Figure 3G shows the profile of uaRNA accumulation from the compilation of a series of 1200 genes with similar expression levels. Likewise, Mof inactivation resulted in accumulation of non-matured U snRNA, reproducing another RNA signature of senescence (Figure 3B, bottom tracts). Consistent with reduced RNA decay, we noted in the Mof KO cells, a significant decrease in the expression of several subunits of the RNA exosome, particularly the catalytic subunit Dis3l, as well as Exosc3, Exosc7, and Exosc9 (Figure 3H). In parallel, and consistent with Mof inactivation driving cells into growth arrest, we noted a clear increase in the expression of the senescence marker Cdkn1a (Figure 3I).

Together, these observations are suggestive of a bidirectional crosstalk between oxidative stress and RNA degradation for the induction of growth arrest. In this model, oxidative stress would cause reduced activity and/or expression of RNA decay enzymes, while reduced RNA decay would induce mitochondrial stress, that in turn would induce production of mtROS and generate oxidative stress. Possibly, this self-sustained mechanism may be a fundamental engine participating in driving cells into senescence.

Activated immune cells accumulate senescence-signature RNAs at a restricted number of genes.

We next wished to investigate whether senescence signature RNAs were also to be detected during normal activation of cellular defence mechanisms. This prompted us to compare the transcriptome of T cells either undergoing activation or enduring oxidative stress. To that end, we re-examined in-house data from Jurkat T cells treated with either PMA, or dieldrin (28). PMA activates PKC, while the pesticide dieldrin was recently shown to induce strong T cell activation *via* activation of both PKC and calcium dependent pathways. As a complement, we also examined unpublished data from the same Jurkat T cells exposed to hydrogen peroxide. All the libraries were prepared simultaneously using the same protocol and all the sequencing reactions were carried out on the same flow cells. Principal component analysis (PCA) confirmed that the H2O2 treatment segregated away from the progressive T cell activation reach respectively with PMA and dieldrin (Fig 4A). The PCA also established that the H2O and DMSO baselines were very similar.

The high depth of the sequencing (100 million reads per sample) ensured detection of rare RNAs. However, as the libraries were poly(A)-selected, we expected to detect uaRNA, but not enhancer RNAs (eRNAs), or U snRNAs. Examination of the 5260 promoters assessed in Figure 1 confirmed the accumulation of auRNAs anticipated from the exposure of the cells to H2O2 (light blue line, Figure 4B). This accumulation was not observed globally in the activated T cells. Yet, in the presence of PMA, strongly activated immediate early genes like *EGR1* abundantly produced uaRNAs at their promoters, covering a region of more than 5Kb. Moreover, we noted that dieldrin, that activated *EGR1* to the same level as did PMA, caused a further accumulation of uaRNAs (Figure 4C, bottom panel). A similar uncoupling between gene expression and uaRNA production was observed at beta actin, a gene stimulated

neither by PMA nor dieldrin (ACTB, Figure 4D). Further examination of the data revealed that additional senescence-signature RNAs had pulled through the polyA selection. This included some immature U RNAs and the stabilized HIST2H2BE 3' UTR (Figure 4E and I).

To increase the robustness of our observations and acquire further evidence for an uncoupling between uaRNA production and gene activity, we next examined an additional set of RNA-seq data from the GM12878 B cell line treated with interferon alpha (29). In these data, as above, we observed accumulation of uaRNAs at the *EGR1* and Actin beta promoters in the absence of a significant activation of these genes (Figure 4G and 4H). In parallel, we observed accumulation of immature U snRNAs and a stabilization of the 3'UTR of HIST2H2BE (Figure 4F and 4J).

Together, these data strongly suggest that accumulation of senescence-signature RNAs is a common step of normal immunity although it occurs only at a limited number of genes and possibly *via* mechanisms different from those at play in senescent cells or cells exposed to oxidative stress.

Serendipitous transcription of SINEs in senescence signature RNAs

As mentioned above, examination of the RNA-seq data from the activated Jurkat cells uncovered an unexpected enrichment of non-polyadenylated RNAs in the poly(A)-selected libraries. Comparing the poly(A)-selected data with data from ribo-depleted libraries generated with the same dieldrin-treated Jurkat cells (28) revealed that poly(A) selection of the non-polyadenylated RNAs was mostly due to the presence of genome-encoded poly(A) tracts (see example of the FOS enhancer Sup. Figure 5A and 5B). Incidentally, in actively transcribed chromatin (euchromatin), (A) tracts are primarily originating from SINE repeats and are required for the retrotransposition of these elements (30). This brought our attention on the presence of SINE sequences in essentially all the senescence-signature RNAs we had examined (see bottom tracts in Figures 1 and 4). In addition, SINE-containing RNAs were previously shown to stimulate secretion of cytokines in B cells (29). Finally, another study has reported an accumulation SINE RNA sequences in senescent cells (12). Together, these observations prompted us to envision that RNAs produced by regulatory elements, including eRNAs and uaRNAs which largely contribute to senescence-signature RNAs, could be a source of SINE-containing RNAs intentionally expressed during inflammatory episodes.

To challenge the possibility of a regulated production of SINE-containing RNAs, we first examined whether there would be a tissue specificity associated with these RNAs. To that end, we extracted all regions annotated as active promoters or enhancers in the 127 tissues mapped by the NIH Roadmap Epigenomics Mapping Consortium (Roadmap Epigenomics Consortium *et al*, 2015). These regions will be referred to as Regulatory Elements (REs). We then estimated the similarity between each of the 127 sets of REs and regions annotated SINEs in RepeatMasker using the Jaccard index. This index is defined as the size of the intersection divided by the size of the union of the sample sets. As the total number of REs varies among the tissues, we also calculated the Jaccard index between the REs from each tissue and randomly selected SINE-free regions (average of thousand iterations). The score shown for each tissue in Figure 5A is the Jaccard index (REs vs. SINEs) divided by the Jaccard index

(REs vs. random). The approach showed that the overlap between PEs and SINEs varied extensively from one tissue to the other, being generally low in embryonic cells and in brain, while remarkably high in a range of immune cells (T cells, B cells, NK cells *etc*.). To finetune this observation, we segregated enhancers from promoters and reiterated the calculation of the Jaccard index on just enhancers. This resulted in a further clustering of immune cells among the top-scoring tissues (Sup. Figure 5D). To improve understanding of the phenomenon, we plotted the average distribution of SINE sequences relative to enhancers and promoters for both top- and bottom-scoring tissues (T cells and neuronal progenitors, respectively). This established that enhancers were peaks of SINEs in T cells while they were valleys of SINEs in the neuronal progenitor cultured cells (Figure 5B). This approach also illustrated that promoters are valleys of SINEs in both tissues (Figure 5C and Sup. Figure 5D). Together, these observations strongly suggesting that cells involve in organismal defence favour the presence of SINE sequences in the neighbourhood of their enhancers and that these SINE sequences get serendipitously transcribed upon activation of the enhancers (see model Figure 5D and actual examples in Sup. Figure 5E and 5F). As for promoters, our observations suggested that, regardless of the tissue, the regulatory elements may produce SINE-containing RNAs only when transcription extends beyond the SINE-free region within which they are positioned. This would be compatible with accumulation of SINE-containing uaRNAs at strongly activated promoters such as the EGR1 promoter during T cell activation (Figure 4C) and at promoters transcribed by a “creeping RNAPII” as reported in cells exposed to oxidative stress (23).

To further document that production SINE-containing RNAs is associated with cellular defence, we took a reversed approach and questioned the function of genes located in the neighbourhood of regulatory elements likely to produce these RNAs. To that end, we performed an intersection between SINEs and positions annotated as sites of transcription initiation (TSS) in at least one of the 975 CAGE libraries of the Fantom5 consortium. We then used GREAT to identify genes located less than 100Kb away from these sites of transcription initiation (enhancers or promoters). PANTHER pathway analysis on these genes clearly identified inflammation and T and B cells as benefitting from these regulatory elements (Figure 5E).

Together, these observations suggest that the production of SINE-containing RNAs is a normal step during the onset cellular defense mechanisms and that regulatory sequences while ensuring enhancer and promoter functions for the genes involved in immunity, also contribute to the production of these RNA species.

Discussion

While senescent cells have many characteristic phenotypes, including the growth arrest, the modified chromatin structure, and secretion of proinflammatory molecules, their transcriptome remains heterogeneous, making difficult their unambiguous identification. Here, we show that a so-far overlooked property of senescent cells is a reduced efficiency of RNA turnover. We find that in all the senescent cells we examined, including five cell lines subject to either oncogene-induced senescence or DNA damage-induced senescence, at least one component of the mRNA decay machinery suffered strongly reduced expression.

In four out of these five types of senescent cells, the deficiency was to be found in the core of the RNA exosome, with frequently multiple subunits being downregulated. In the nucleus, this complex degrades uaRNAs, replication-dependent histone mRNAs, eRNAs, snRNAs, and snoRNAs. It also eliminates cryptic transcripts, misprocessed RNAs, and transposons (17). In the cytoplasm, the RNA exosome is required for quality control in the context of nonsense-mediated decay (NMD) and more generally for the turn-over of mRNAs (31). The fact that senescent melanocytes showed reduced expression of three factors involved in turnover of polyadenylated mRNAs in the cytoplasm, while showing no decrease in the expression of core components of the RNA exosome bring us to suggest that it is the cytoplasmic RNA exosome that is critical in senescence. This would be compatible with the numerous splice variants, targets of NMD, that accumulate in the senescent cells. It would also be compatible with an earlier study of cells subject to oxidative stress, showing that a large fraction of the uaRNAs accumulating in these cells are also detected in the polysomes (22). However, the downregulation of multiple RNA exosome subunits and the accumulation of immature snRNAs in the senescent cells would favour a targeting of both the cytoplasmic and nuclear versions of the complex.

Another conclusion from our study is that oxidative stress and RNA turnover are associated in a feed-back loop. Earlier studies have documented that the accumulation of uaRNAs and eRNAs upon acute exposure of cells to H2O2 was caused by a defective RNAPII termination, causing these RNAs to be longer and more abundant. We show here that this phenomenon is further amplified by reduced RNA turn-over documented by the accumulation of multiple RNA species normally degraded by the RNA exosome and by the reduced expression of several genes encoding RNA exosome subunits. Similarly, mitochondrial suffering induced by inactivation of MOF in a mouse model results in reduced expression of core components of the RNA exosome and accumulation of RNA species that this complex degrades.

Reciprocally, inactivation of a core component of the RNA exosome, namely ExoSC3, resulted in reduced expression of mitochondrial genes and increased expression of several markers of senescence. Interestingly, medical data partially recapitulate these observations. Indeed, patients suffering from pontocerebellar hypoplasia, a disease affecting the development of the brain and due to a mutation in the *EXOSC3* gene were also described as showing signs of mitochondrial dysfunction (26). In parallel, patients with mutations in EXOSC2 are subject to premature ageing (32). These observations raise the question of the potential role of undesired RNA accumulation in driving and maintaining the senescent phenotype.

Failure to degrade RNA species prone to form RNA:DNA hybrids is a source of DNA damage and this phenomenon is a well-documented link between RNA and cellular senescence (33). Another mechanism mentioned in the introduction is the accumulation of transcripts encoded by transposons that, once retrotranscribed into cDNA, become triggers of an interferon response to promote senescence (6). Our observations lead us to suggest another alternative, namely that accumulation of certain RNA species drives production of mitochondrial reactive oxygen species that nurtures both the inflammatory response and the reduced RNA turnover. This model is sustained by the extensive impact that strong oxidative stress has on the accumulation of the signature RNA species. It is also compatible with the more restricted production of senescence signature RNAs upon activation of T and B cells, suggesting that the production of these RNAs are a normal step in the innate immune

response aimed at promoting mitochondria-mediated defence mechanisms. The accumulation of antibacterial noncoding RNAs upon Salmonella infection may be an illustration of this (34).

The mechanism allowing the signature RNAs to affect mitochondrial activity remains an open question. Examination of the sequence of the accumulating RNAs revealed that they were rich in SINE/Alu sequences, a family of retrotransposons very abundantly present in euchromatin. These sequences have previously been shown to stimulate secretion of cytokines via a mechanism blocked by inhibitors of toll-like receptors (TLRs) 3, 7, and 8, all of which recognize RNA (29). Among these, at least TLR3 is known to communicate directly with the mitochondria (35). Following the same logic, by examining promoters and enhancers throughout human tissues, we find that immune cells display a clear positive selection of SINE/Alus in their regulatory sequences. This strongly suggests that transient production of transcription encoding Alu sequences is beneficial for the immune reaction. Extrapolation of this concept lead us to suggest that the chronic accumulation of Alu-containing RNAs due to reduced expression of components of RNA decay machineries could be a major driver of the inflammatory phenotype associated with cellular senescence (model in Figure 6).

Acknowledgements

We thank S. Azebi for technical assistance and M. Ricchetti for critical reading of the manuscript. The work was supported by grants from Institut Pasteur, LABEX REVIVE, and Agence Nationale de la Recherche.

Material and methods

High-throughput RNA sequencing

Jurkat E6-1 cells purchased from ATCC were cultured in RPMI-1640 with 10% decomplemented fetal bovine serum (FBS) and 100 U ml^{-1} penicillin–streptomycin at 37°C in a 5% CO_2 incubator. Cells were treated with 0.2mM hydrogen peroxide for 30 min before harvesting the RNA. Stranded libraries of cDNA were prepared by random priming followed by enrichment in poly(dA) with an oligo(dT) resin. A minimum of 30-Gb sequencing was obtained for each sample with reads of 150 bases. Poly(dA)-enriched libraries were constructed and sequenced together with those described in (28). GEO accession number: GSE138290.

Data download

RNA-seq raw fastq files were downloaded from the Gene Expression Omnibus (GEO) on the NCBI database with the SRA toolkit (http://ncbi.github.io/sra-tools/). The files were retrieved from GSE111167, GSE55172, GSE72420, GSE77784, GSE81662, GSE85085, GSE100535 and GSE108278. The fastq files from the analysis E-MTAB-5403 were downloaded from ArrayExpress on the EBI database.

Mapping

For the mapping, SHRiMP were used (v2.2.3) (36) for the dataset GSE55172 (colorspace reads) (parameters: -o 1 --max-alignments 10 --strata) while for the others, mapping were done with STAR (v2.6.0b) (37) (parameters: --outFilterMismatchNmax 1 --outSAMmultNmax 1 --outMultimapperOrder Random --outFilterMultimapNmax 30). Mapping were done against the reference human genome (hg19 homo sapiens primary assembly from Ensembl) for our Jurkat dataset (GSE111167 and GSE138290), EBI dataset, GSE55172, GSE72420, GSE81662, GSE85085, GSE108278 and against the reference mouse genome (mm9 mus musculus primary assembly from Ensembl) for the GSE77784 and GSE100535). The SAM files were then converted to the BAM format and sorted by coordinate with samtools (v1.7) (38).

Data observations

Bigwigs files were generated with bamCoverage (parameter: --normalizeUsing CPM) from Deeptools (v3.1.3) (39). All observations were done using the Integrative Genomics Viewer software (IGV) (40).

Differential gene expression and splicing analysis:

The package Subread (v1.28.1) (41) for R (v3.4.3) were used to count the uniquely mapped reads based on a gtf annotation file for hg19 or mm9 from Ensembl. Then the package DESeq2 (v1.18.1) (42) were used to make the differential gene expression analysis and principal component analysis (PCA). P-values from the differential gene expression test were adjusted for multiple testing according to the Benjamini and Hochberg procedure. Only genes with an adjusted p-value lower than 0.05 were considered differentially expressed. GO term analysis were performed on these differentially expressed genes with Enrichr (43). Analysis of splicing was performed with AltAnalyze V2.0.9 (44).

Heatmaps, profiles, and Jaccard index:

Reads inside upstream gene regions and downstream U snRNA regions were quantified using featureCounts (v1.6.1) from the Subread suite (41).

Then, from these counts, matrices were generated with the tool computeMatrix reference-point (parameter: --referencePoint TSS for the observations of the regions upstream of the genes or --referencePoint TES for the observations of the downstream regions of U snRNA). Profiles were obtained using plotProfile (parameter: --perGroup) and heatmaps using plotHeatmap (default paramaters) from the Deeptools suite (39). Jaccard index was calculated as in (28).

REFERENCES

1. Rodier F, Campisi J. Four faces of cellular senescence. The Journal of Cell Biology. 2011 Feb 21;192(4):547–56.

2. Ben-Porath I, Weinberg RA. The signals and pathways activating cellular senescence. The International Journal of Biochemistry & Cell Biology. 2005 May;37(5):961–76.

3. Salminen A, Kauppinen A, Kaarniranta K. Emerging role of NF-κB signaling in the induction of senescence-associated secretory phenotype (SASP). Cellular Signalling. Elsevier Inc; 2012 Apr 1;24(4):835–45.

4. Dou Z, Ghosh K, Vizioli MG, Zhu J, Sen P, Wangensteen KJ, Simithy J, Lan Y, Lin Y, Zhou Z, Capell BC, Xu C, Xu M, Kieckhaefer JE, Jiang T, Shoshkes-Carmel M, Tanim Al KMA, Barber GN, Seykora JT, Millar SE, Kaestner KH, Garcia BA, Adams PD, Berger SL. Cytoplasmic chromatin triggers inflammation in senescence and cancer. Nature. Nature Publishing Group; 2017 Oct 19;550(7676):402–6.

5. Takahashi A, Loo TM, Okada R, Kamachi F, Watanabe Y, Wakita M, Watanabe S, Kawamoto S, Miyata K, Barber GN, Ohtani N, Hara E. Downregulation of cytoplasmic DNases is implicated in cytoplasmic DNA accumulation and SASP in senescent cells. Nat Commun. Springer US; 2018 Mar 16;:1–12.

6. Cecco M, Ito T, Petrashen AP, Elias AE, Skvir NJ, Criscione SW, Caligiana A, Brocculi G, Adney EM, Boeke JD, Le O, jour CBX, Ambati J, Ambati K, Simon M, Seluanov A, Gorbunova V, Slagboom PE, Helfand SL, Neretti N, Sedivy JM. L1 drives IFN in senescent cells and promotes age-associated inflammation. Nature. Springer US; 2019 Jul 2;:1–33.

7. Katlinskaya YV, Katlinski KV, Yu Q, Ortiz A, Beiting DP, Brice A, Davar D, Sanders C, Kirkwood JM, Rui H, Xu X, Koumenis C, Diehl JA, Fuchs SY. Suppression of Type I Interferon Signaling Overcomes Oncogene-Induced Senescence and Mediates Melanoma Development and Progression. CELREP. ElsevierCompany; 2016 Apr 5;15(1):171–80.

8. Du WW, Yang W, Liu E, Yang Z, Dhaliwal P, Yang BB. Foxo3 circular RNA retards cell cycle progression via forming ternary complexes with p21 and CDK2. Nucleic Acids Res. 2016 Apr 7;44(6):2846–58.

9. Du WW, Yang W, Chen Y, Wu Z-K, Foster FS, Yang Z, Li X, Yang BB. Foxo3 circular RNA promotes cardiac senescence by modulating multiple factors associated with stress and senescence responses. Eur Heart J. 2016 Feb 11;113((Pt 20)):ehw001–11.

10. Lazorthes S, Vallot C, Briois S, Aguirrebengoa M, Thuret J-Y, St Laurent G, Rougeulle C, Kapranov P, Mann C, Trouche D, Nicolas E. A vlincRNA participates in senescence maintenance by relieving H2AZ-mediated

repression at the INK4 locus. Nat Commun. Nature Publishing Group; 2015 Jan 20;6(1):5971–16. PMCID: PMC4309439

11. Sudmant PH, Lee H, Dominguez D, Heiman M, Burge CB. Widespread Accumulation of Ribosome-Associated Isolated 3′ UTRs in Neuronal Cell Populations of the Aging Brain. Cell Rep. 2018 Nov 27;25(9):2447–2456.e4. PMCID: PMC6354779

12. Wang J, Geesman GJ, Hostikka SL, Atallah M, Blackwell B, Lee E, Cook PJ, Pasaniuc B, Shariat G, Halperin E, Dobke M, Rosenfeld MG, Jordan IK, Lunyak VV. Inhibition of activated pericentromeric SINE/Alu repeat transcription in senescent human adult stem cells reinstates self-renewal. Cell Cycle. 2014 Oct 28;10(17):3016–30.

13. Wang K, Di Wu, Zhang H, Das A, Basu M, Malin J, Cao K, Hannenhalli S. Comprehensive map of age- associated splicing changes across human tissues and their contributions to age-associated diseases. Sci Rep. Springer US; 2018 Jul 13;:1–12.

14. Cao K, Blair CD, Faddah DA, Kieckhaefer JE, Olive M, Erdos MR, Nabel EG, Collins FS. Progerin and telomere dysfunction collaborate to trigger cellular senescence in normal human fibroblasts. J. Clin. Invest. American Society for Clinical Investigation; 2011;121(7):2833.

15. Fujita K, Mondal AM, Horikawa I, Nguyen GH, Kumamoto K, Sohn JJ, Bowman ED, Mathe EA, Schetter AJ, Pine SR, Ji H, Vojtesek B, Bourdon J-C, Lane DP, Harris CC. p53 isoforms Delta133p53 and p53beta are endogenous regulators of replicative cellular senescence. Nat Cell Biol. Nature Publishing Group; 2009 Sep;11(9):1135–42. PMCID: PMC2802853

16. Miao Z-F, Wu J-H, Wang Z-N, Zhao T-T, Xu H-M, Song Y-X, Xing Y-N, Huang J-Y, Zhang J-Y, Liu X-Y, Xu H, Xu Y-Y. Endoglin overexpression mediates gastric cancer peritoneal dissemination by inducing mesothelial cell senescence. Hum. Pathol. 2016 May;51:114–23.

17. Ogami K, Chen Y, Manley J. RNA Surveillance by the Nuclear RNA Exosome: Mechanisms and Significance. ncRNA. 2018 Mar;4(1):8–21.

18. Lau L, Porciuncula A, Yu A, Iwakura Y, David G. Uncoupling the senescence-associated secretory phenotype from cell cycle exit via IL-1 inactivation unveils its pro-tumorigenic role. Mol Cell Biol. 2019 Apr 15;:1–47.

19. Hernandez-Segura A, de Jong TV, Melov S, Guryev V, Campisi J, Demaria M. Unmasking Transcriptional Heterogeneity in Senescent Cells. Curr Biol. 2017 Sep 11;27(17):2652–4. PMCID: PMC5788810

20. Muniz L, Deb MK, Aguirrebengoa M, Lazorthes S, Trouche D, Nicolas E. Control of Gene Expression in Senescence through Transcriptional Read-Through of Convergent Protein-Coding Genes. CELREP. ElsevierCompany; 2017 Nov 28;21(9):2433–46.

21. Schlackow M, Nojima T, Gomes T, Dhir A, Carmo-Fonseca M, Proudfoot NJ. Distinctive Patterns of Transcription and RNA Processing for Human lincRNAs. Mol Cell. Elsevier Inc; 2017 Jan 5;65(1):25–38.

22. Giannakakis A, Zhang J, Jenjaroenpun P, Nama S, Zainolabidin N, Aau MY, Yarmishyn AA, Vaz C, Ivshina AV, Grinchuk OV, Voorhoeve M, Vardy LA, Sampath P, Kuznetsov VA, Kurochkin IV, Guccione E. Contrasting expression patterns of coding and noncoding parts of the human genome upon oxidative stress. Sci Rep. Nature Publishing Group; 2015 May 29;5(1):9737. PMCID: PMC4448690

23. Nilson KA, Lawson CK, Mullen NJ, Ball CB, Spector BM, Meier JL, Price DH. Oxidative stress rapidly stabilizes promoter-proximal paused Pol II across the human genome. Nucleic Acids Res. 2017 Aug 18. PMCID: PMC5737879

24. Blasius M, Wagner SA, Choudhary C, Bartek J, Jackson SP. A quantitative 14-3-3 interaction screen connects the nuclear exosome targeting complex to the DNA damage response. Genes & Development. 2014 Sep 16;28(18):1977–82.

25. Chiu AC, Suzuki HI, Wu X, Mahat DB, Kriz AJ, Sharp PA. Transcriptional Pause Sites Delineate Stable Nucleosome-Associated Premature Polyadenylation Suppressed by U1 snRNP. Mol Cell. Elsevier Inc; 2018 Feb 15;69(4):648–663.e7. PMCID: PMC6175280

26. Schottmann G, Picker-Minh S, Schwarz JM, Gill E, Rodenburg RJT, Stenzel W, Kaindl AM, Schuelke M. Recessive mutation in EXOSC3 associates with mitochondrial dysfunction and pontocerebellar hypoplasia. Mitochondrion. Elsevier; 2017 Nov 1;37:46–54.

27. Chatterjee A, Seyfferth J, Lucci J, Gilsbach R, Preissl S, Böttinger L, Mårtensson CU, Panhale A, Stehle T, Kretz O, Sahyoun AH, Avilov S, Eimer S, Hein L, Pfanner N, Becker T, Akhtar A. MOF Acetyl Transferase Regulates Transcription and Respiration in Mitochondria. Cell. 2016 Oct 20;167(3):722–3.

28. Azebi S, Batsché E, Michel F, Kornobis E, Muchardt C. Expression of endogenous retroviruses reflects increased usage of atypical enhancers in T cells. EMBO J. 2019 May 8.

29. Hung T, Pratt GA, Sundararaman B, Townsend MJ, Chaivorapol C, Bhangale T, Graham RR, Ortmann W, Criswell LA, Yeo GW, Behrens TW. The Ro60 autoantigen binds endogenous retroelements and regulates inflammatory gene expression. Science. 2015 Oct 23;350(6259):455–9. PMCID: PMC4691329

30. Dewannieux M, Heidmann T. Role of poly(A) tail length in Alu retrotransposition. Genomics. 2005 Sep;86(3):378–81.

31. Łabno A, Tomecki R, Dziembowski A. Cytoplasmic RNA decay pathways - Enzymes and mechanisms. BBA - Molecular Cell Research. Elsevier B.V; 2016 Dec 1;1863(12):3125–47.

32. Di Donato N, Neuhann T, Kahlert A-K, Klink B, Hackmann K, Neuhann I, Novotna B, Schallner J, Krause C, Glass IA, Parnell SE, Benet-Pages A, Nissen AM, Berger W, Altmüller J, Thiele H, Weber BHF, Schrock E, Dobyns WB, Bier A, Rump A. Mutations in EXOSC2are associated with a novel syndrome characterised by retinitis pigmentosa, progressive hearing loss, premature ageing, short stature, mild intellectual disability and distinctive gestalt. Journal of Medical Genetics. 2016 May 24;53(6):419–25.

33. Nojima T, Tellier M, Foxwell J, de Almeida CR, Tan-Wong SM, Dhir S, Dujardin G, Dhir A, Murphy S, Proudfoot NJ. Deregulated Expression of Mammalian lncRNA through Loss of SPT6 Induces R-Loop Formation, Replication Stress, and Cellular Senescence. Mol Cell. Elsevier Inc; 2018 Dec 20;72(6):970–7.

34. Imamura K, Takaya A, Ishida YI, Fukuoka Y, Taya T, Nakaki R, Kakeda M, Imamachi N, Sato A, Yamada T, Onoguchi Mizutani R, Akizuki G, Tanu T, Tao K, Miyao S, Suzuki Y, Nagahama M, Yamamoto T, Jensen TH, Akimitsu N. Diminished nuclear RNA decay upon Salmonellainfection upregulates antibacterial noncoding RNAs. EMBO J. 2018 Jul 2;37(13):e97723–15.

35. Djafarzadeh S, Vuda M, Takala J, Ochs M, Jakob SM. Toll-like receptor-3-induced mitochondrial dysfunction in cultured human hepatocytes. Mitochondrion. Elsevier B.V. and Mitochondria Research Society; 2011 Jan 1;11(1):83–8.

36. David M, Dzamba M, Lister D, Ilie L, Brudno M. SHRiMP2: sensitive yet practical SHort Read Mapping. Bioinformatics. 2011 Apr 1;27(7):1011–2.

37. Dobin A, Davis CA, Schlesinger F, Drenkow J, Zaleski C, Jha S, Batut P, Chaisson M, Gingeras TR. STAR: Ultrafast universal RNA-seq aligner. Bioinformatics. 2013 Jan 1;29(1):15–21. PMCID: PMC3530905

38. Li H, Handsaker B, Wysoker A, Fennell T, Ruan J, Homer N, Marth G, Abecasis G, Durbin R, 1000 Genome Project Data Processing Subgroup. The Sequence Alignment/Map format and SAMtools. Bioinformatics. 2009 Aug 15;25(16):2078–9. PMCID: PMC2723002

39. Ramirez F, Ryan DP, Grüning B, Bhardwaj V, Kilpert F, Richter AS, Heyne S, Dündar F, Manke T. deepTools2: a next generation web server for deep-sequencing data analysis. Nucleic Acids Res. 2016 Jul 8;44(W1):W160–5. PMCID: PMC4987876

40. Robinson JT, Thorvaldsdóttir H, Winckler W, Guttman M, Lander ES, Getz G, Mesirov JP. Integrative genomics viewer. Nature Publishing Group. Nature Publishing Group; 2011 Jan;29(1):24–6. PMCID: PMC3346182

41. Liao Y, Smyth GK, Shi W. featureCounts: an efficient general purpose program for assigning sequence reads to genomic features. Bioinformatics. 2014 Mar 27;30(7):923–30.

42. Love MI, Huber W, Anders S. Moderated estimation of fold change and dispersion for RNA-seq data with DESeq2. Genome Biol. BioMed Central; 2014;15(12):550–21. PMCID: PMC4302049

43. Kuleshov MV, Jones MR, Rouillard AD, Fernandez NF, Duan Q, Wang Z, Koplev S, Jenkins SL, Jagodnik KM, Lachmann A, McDermott MG, Monteiro CD, Gundersen GW, Ma'ayan A. Enrichr: a comprehensive gene set enrichment analysis web server 2016 update. Nucleic Acids Res. 2016 Jul 4;44(W1):W90–7. PMCID: PMC4987924

44. Emig D, Salomonis N, Baumbach J, Lengauer T, Conklin BR, Albrecht M. AltAnalyze and DomainGraph: analyzing and visualizing exon expression data. Nucleic Acids Res. 2010 Jul;38(Web Server issue):W755–62. PMCID: PMC2896198

45. Lloret-Llinares M, Mapendano CK, Martlev LH, Lykke-Andersen S, Jensen TH. Relationships between PROMPT and gene expression. RNA biology. Taylor & Francis; 2016 Jan 30;13(1):6–14.

Figure legends:

Figure 1: Cellular senescence is associated with reduced RNA turnover.

(A-B) RNA-seq data from IMR90 human fibroblasts induced to senesce via activation of oncogene Ras (18). Samples (n=4) had been collected at day 0 (growing phase), day 4 (beginning of SASP induction) and day 10 (senescent phase) of Ras induction. All data was analyzed for alternative splicing using AltAnalyze and differential gene expression was estimated with DESeq2. (A) shows the number of splicing events diverging between days 0 and 4, and between 0 and 10, classified in indicated categories. (B) shows variations in expression levels of the indicated genes. For each condition, n=4. Differential gene expression was estimated with DESeq2, data are presented as the mean of the fold change. *** and ** indicate p-values below 0.001 and 0.01 respectively. (C, E, I, K) RNA-seq data from WI38 hTERT RAF1-ER human fibroblasts either proliferating (n=1) or driven into senescence (n=1) by induction of RAF1-ER (10) and RNA-seq data from HeLa cells transfected either with siLuc (control, n=1) or siEXOSC3 (n=1) (21) were aligned on Hg19 and visualized with IGV. Black arrows indicate the orientation of the gene. Blue arrows and bars indicate regions of interest. Figures inside each panel represent the ratio between the read-counts in the red region over the green region located under the genome coordinates. (D) Schematic representation of divergent transcription at promoters. Green line represents pre-mRNA, blue line, normal accumulation of uaRNAs, red line, accumulation of uaRNAs in senescent cells. (F-H) At 5260 promoters not overlapping with coding regions of any gene, reads were counted on a region of 1500 nucleotides upstream of the transcription start site (TSS) in either the WI38 hTERT RAF1-ER or the HeLa cells. Promoters displaying an accumulation of reads increased more than 2-fold between in senescent versus proliferating cells and aligning with more than 10 reads were listed in Sup. Table 1A after manual curation. Promoters satisfying the same criteria between siLuc (control) or siEXOSC3 knock-down are listed in Sup. Table 1B. Number of overlaps between the lists is indicated in a Venn diagram panel (F). (G) Total number of reads detected at the 5260 promoters in either proliferating or senescent WI38 hTERT RAF1-ER cells. (H) Average profile of read distribution along the 5260 promoters in proliferating and senescent WI38 hTERT RAF1-ER cells. (J) Heatmap illustrating increased accumulation of non-maturated U snRNAs in senescent vs. proliferating WI38 hTERT RAF1-ER cells. The U snRNAs are also listed in Sup. Table 1C.

Sup. Figure 1: Cellular senescence is associated with reduced RNA turnover.

(A-F) RNA-seq data where HCA-2 (fibroblasts), keratinocytes, or melanocytes had been exposed to ionizing radiation. RNA had been harvested 4, 10, or 20 days later (n=5 for each cell type and time point) (19). All data was analyzed for alternative splicing using AltAnalyze and differential gene expression was estimated with DESeq2. (A, C, E) show the number of splicing events diverging between days 0 and 4, 0 and 10, and 0 and 20, classified in indicated categories. (B, D, F) shows variations in expression levels of the indicated genes. For each condition, n=5. Differential gene expression was estimated with DESeq2, data are presented as the mean of the fold change. Blue arrows indicate a significant decrease (p-values below 0.001) relative to day 0 observed in all 3 measures (4, 10, and 20 days). (G) Differential gene expression was estimated with DESeq2 on RNA-seq data from WI38 hTERT RAF1-ER human

fibroblasts either proliferating (n=1) or driven into senescence (n=1) by induction of RAF1-ER (10). Data are presented as the fold change. (H-I) RNA-seq data from WI38 hTERT RAF1-ER human fibroblasts either proliferating or driven into senescence by induction of RAF1-ER (10) and RNA-seq data from HeLa cells transfected either with siLuc (control) or siEXOSC3 (21) were aligned on Hg19 and visualized with IGV genome browser.

Sup Table 1A: List of genes accumulating uaRNAs 2-fold more in senescent as compared to proliferating Wi38 cells.

Sup Table 1B: List of genes accumulating uaRNAs 2-fold more in EXOSC3 KD as compared to WT HeLa cells.

Sup Table 1C: List of snRNA genes accumulating downstream reads 2-fold more in senescent as compared to proliferating Wi38 cells.

Figure 2: Cells exposed to oxidative stress share signature RNAs with senescent cells.
(A, B, C, E) RNA-seq data from either BJ or MRC5 human fibroblasts having been exposed to 0.2mM H2O2 for the indicated times (one sample per time point) were aligned on Hg19 (22). They were then compared to senescent WI38 hTERT RAF1-ER cells from Figure 1 using the IGV genome browser. Blue lines and arrows indicate regions of interest. Figures inside each panel represent the ratio between the read-counts in the red region over the green region located under the genome coordinates. (D) Heatmap illustrating increased accumulation of non-maturated U snRNAs in BJ cells exposed to H2O2 for the indicated times. The U snRNAs are also listed in Sup. Table 2. (F-G) Differential gene expression was estimated with DESeq2. Histograms indicate the fold change obtained for the indicated genes (n=1 for each time point).

Sup. Table 2: List of snRNA genes accumulating downstream reads 2-fold more in H2O2-treated as compared to untreated BJ cells.

Figure 3: Inactivation of the RNA exosome results deregulates mitochondrial genes and induce a senescent phenotype.
(A-B) Mouse ES cells inactivated for Exosc3 and rescued with a dox-inducible exogenous Exosc3 expression system had been grown for 3 days in the absence or in the presence of dox then analyzed by RNA-seq (2 dox+ and 2 dox-) (25). In another study, mouse cardiomyocytes either WT (n=4) or inactivated for the Mof histone acetylase (n=3) were analyzed by RNA-seq (27). These two data sets were aligned on mouse genome mm9 and examined using the IGV genome browser. (C-F, H-I) Differential gene expression in both studies was estimated with DESeq2. (C, E, F) GO term analysis of genes affected 2-fold or more upon Exosc3 KO was carried out with Enrichr. (D, H-I) Histograms show variations of the indicated genes. ***, **, and * indicate p-values below 0.001, 0.01, and 0.05 respectively. (G) Average profile of read distribution along the promoters of 1200 genes with similar expression levels in either WT or Mof KO cardiomyocytes.

Sup. Table 3: differentially regulated genes associated with the GO terms in Figure 3 panel C, E, and F.

Figure 4: Immune cell activation results in the production of senescence-signature RNAs

(A) Jurkat T cells were exposed to either DMSO, DMSO and 100uM PMA, DMSO and 100uM dieldrin (28) or exposed to 0.2mM H2O2 in water for 30 min (n=3 for each condition). Libraries of cDNA were poly(A)-enriched and analyzed by RNA-seq. Reads were aligned on human genome Hg19, differential gene expression was estimated with DESeq2 and used for principal component analysis. (B) Average profile of read distribution along a set of 5260 promoters in the indicated conditions. (C-E, I) Visualization of the indicated loci in IGV genome browser. (F,G-H, J) The EBV-immortalized B cell line GM12878 had been treated or not with IFNa 1000 U/ml for 6 hours, and libraries prepared with ribo-depletion followed by RNA-seq (n=2 for each condition). Reads were aligned on human genome Hg19 and indicated loci visualized using the IGV genome browser. Figures inside each panel represent the ratio between the read-counts in the red region over the green region located under the genome coordinates.

Figure 5: Evidence for a regulated production of SINE-containing RNAs in cells involved in immune defense.

(A) Comparison of regions annotated “SINE” in RepeatMasker with the regions annotated TssA, TssAFlnk, Enh, EnhG, TssBiv, or EnhBiv in the 15 core marks model of the Epigenomic Roadmap consortium (referred to as REs for Regulatory Elements). For each tissue, the Jaccard index comparing REs to SINEs is divided by the average Jaccard index (1000 iterations) obtained when comparing REs to randomly selected genomic locations (of the same sizes as the SINEs). Only the 10 tissues with the highest and the lowest score are shown. (B-C) Profile reporting the position of regions annotated “SINE” in RepeatMasker relative to enhancers or promoters from the indicated tissues. (C) A graphic interpretation of the positioning of enhancers relative SINE sequences in the indicated tissues. (E) PANTHER pathways associated with genes located 100 kb or less from a region annotated “SINE” in RepeatMasker and overlapping with a CAGE peak as defined by the FANTOM5 consortium.

Sup. Figure 5: Evidence for a regulated production of SINE-containing RNAs in cells involved in immune defense.

(A) Jurkat T cells were exposed to either DMSO, DMSO and 100uM PMA, DMSO and 100uM dieldrin (28) or exposed to 0.2mM H2O2 in water for 30 min (n=3 for each condition). Libraries of cDNA were poly(A)-enriched and analyzed by RNA-seq. Reads were aligned on human genome Hg19, differential gene expression was estimated with DESeq2. An enhancer upstream of the FOS gene was visualization in IGV genome browser. Note the uncoupling between accumulation of eRNAs and that of FOS mRNA in cells treated with H202. All tracks in each panel are at the same scale. On the top panel, the scale is adjusted for best visualization of the FOS mRNA; on the bottom panel, the scale is adjusted for best visualization of the eRNAs. (B) eRNAs containing genome-encoded (A)-tracts: RNA-seq data from Jurkat T cells were exposed to either DMSO, or DMSO and 100uM dieldrin as in (A). RNA was then harvested and libraries were constructed using depletion of ribosomal RNA instead of poly(A) enrichment (28). The enhancer of the FOS gene examined in (A) was visualized in IGV, comparing the outcome of the RNA-seq either using depletion of ribosomal RNA (top tracks) or poly(A)-enrichment (bottom tracks). Note that poly(A) selection does not eliminate the left arm of this site of divergent transcription although eRNA are not polyadelynated. The retention of the eRNAs from the left arm through the poly(A) selection is consistent

with the presence in the sequence of the eRNAs of genome-encoded (A)-tracts originating from Alu sequences (red arrow). The region covered by the right arm is devoid of (A)-tracts (blue arrow). (C) Profile reporting the position of regions annotated "SINE" in RepeatMasker relative to enhancers or promoters from neuronal progenitor cells. (D) Comparison of regions annotated "SINE" in RepeatMasker with the regions annotated Enh in the 15 core marks model of the Epigenomic Roadmap consortium (referred to as REs for Regulatory Elements). For each tissue, the Jaccard index comparing REs to SINEs is divided by the average Jaccard index (1000 iterations) obtained when comparing REs to randomly selected genomic locations (of the same sizes as the SINEs). (E-F) Examples of enhancers active in immune cells and overlapping with SINEs visualized in the browser of Roadmap epigenomics project (https://egg2.wustl.edu/roadmap/). Yellow and red areas carry enhancer and promoter marks respectively. The bottom track show repeated DNA sequences with SINE sequences indicated in red.

Figure 6: Model: SINE-containing RNAs as a driver of the sterile inflammation associated with cellular senescence.
An initial pro-inflammatory or stress signal (including DNA damage) triggers production of abundant and elongated uaRNAs that, because of their abundancy, will at least partially escape degradation by the RNA exosome. The uaRNAs get exported to the cytoplasm (22), possibly stabilized by the poly(A) tracts provided by the SINE sequences. In the cytoplasm, SINE sequences get detected by TLR3 or TLR7 (29). Activation of these RNA receptors results mitochondrial dysfunction (35). This results in production of mitochondrial reactive oxygen species (mtROS) that hampers the RNA exosome activity first via oxidation of the subunits or via activation of stress-related kinases (24). Later, upon prolonged oxidative stress, transcription of RNA exosome subunits is turned down, possibly as a consequence of reduced TBP recruitment or increased DNA methylation at their promoters (45).

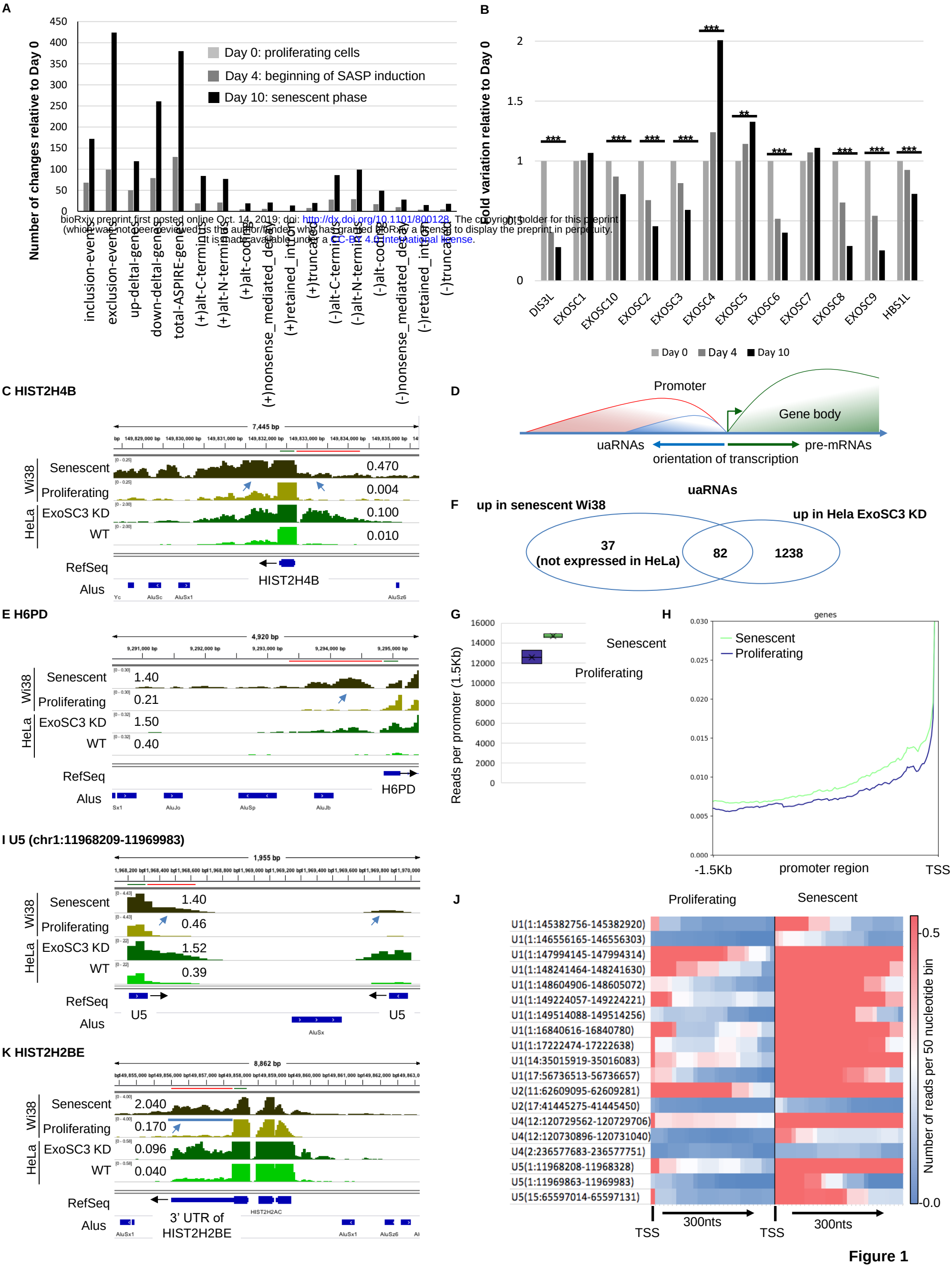

Figure 1

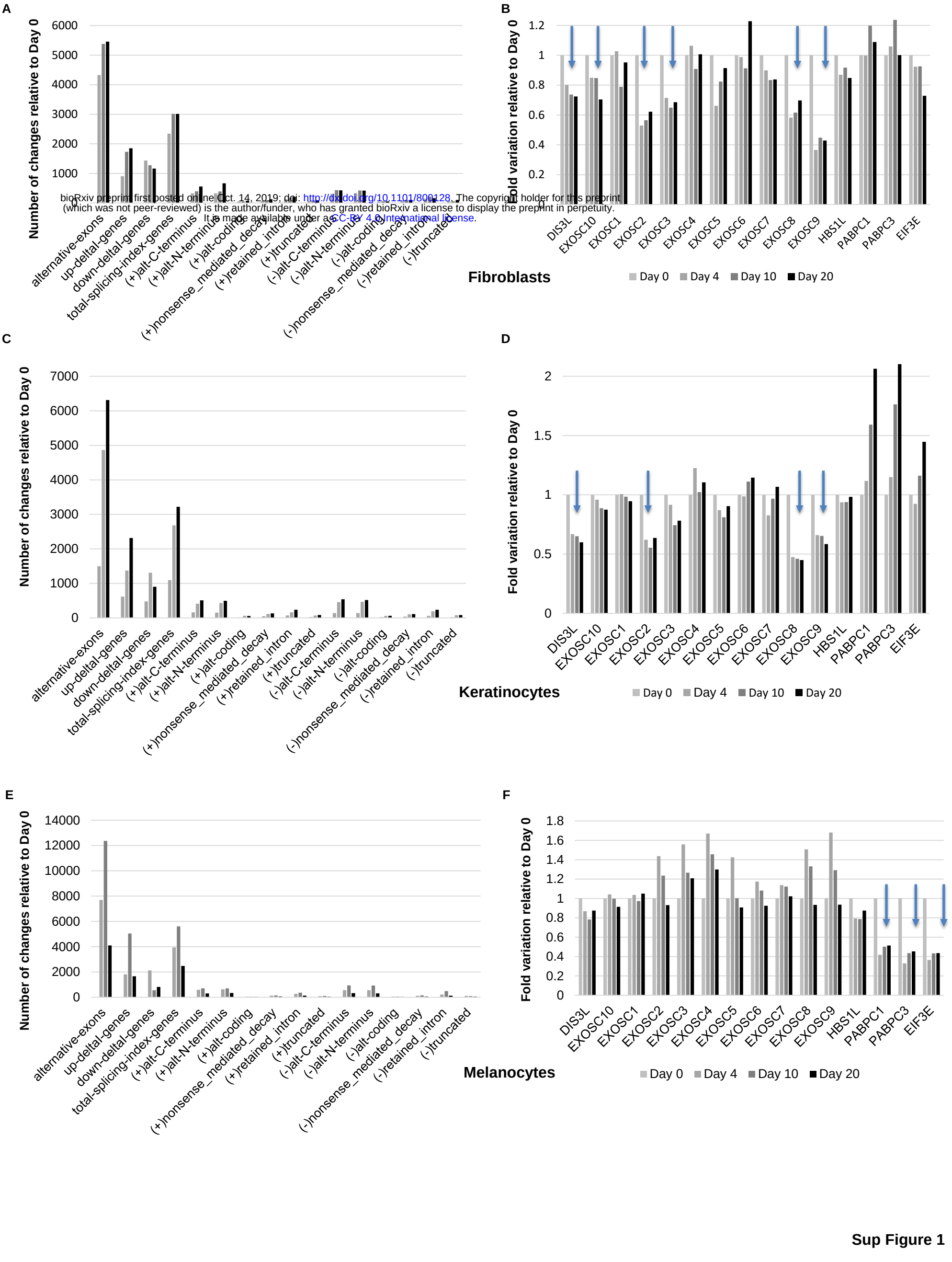

Sup Figure 1

G

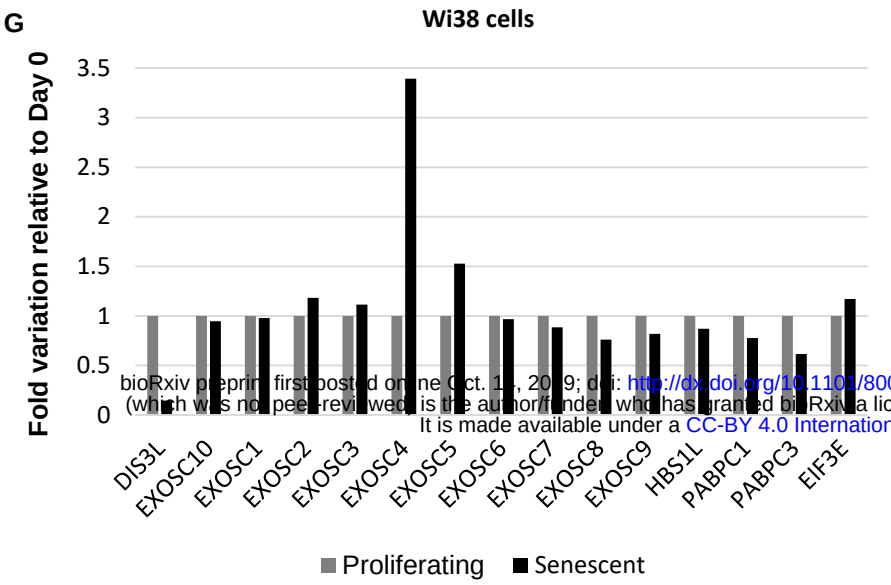

H HIST2H4B – scaled on gene body

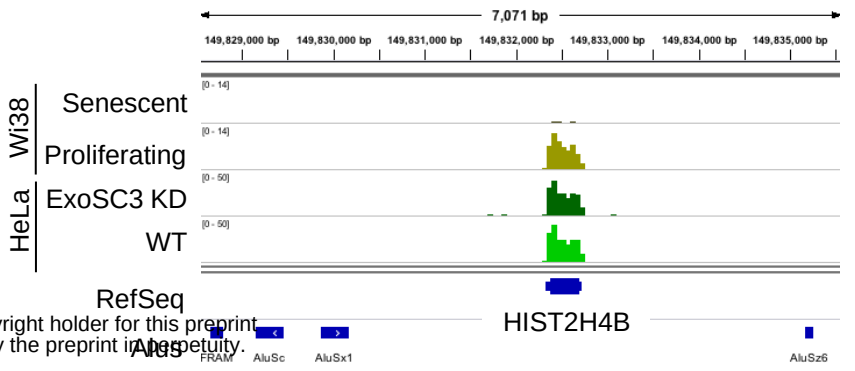

I HIST1H3D and HIST1H2BF

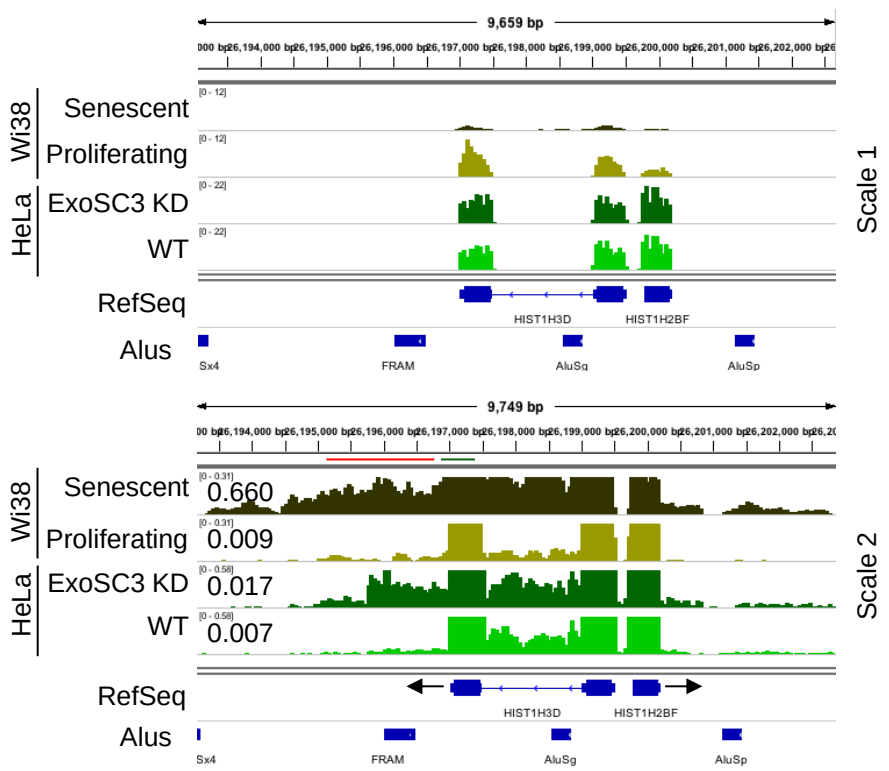

Sup Figure 1

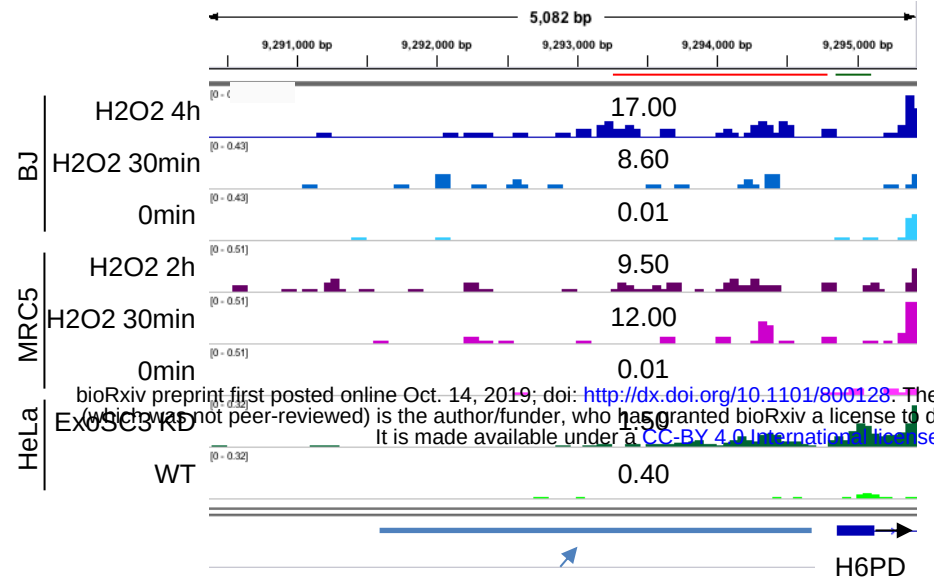

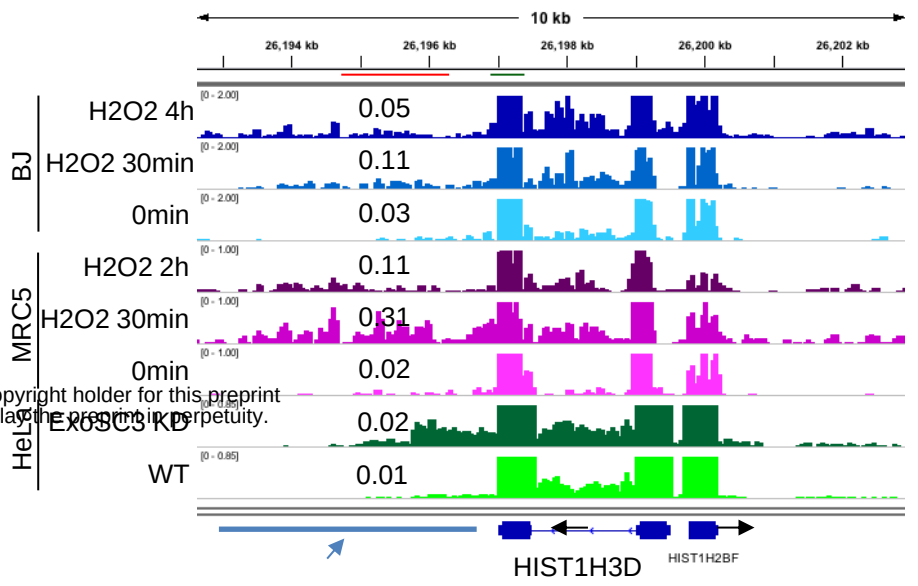

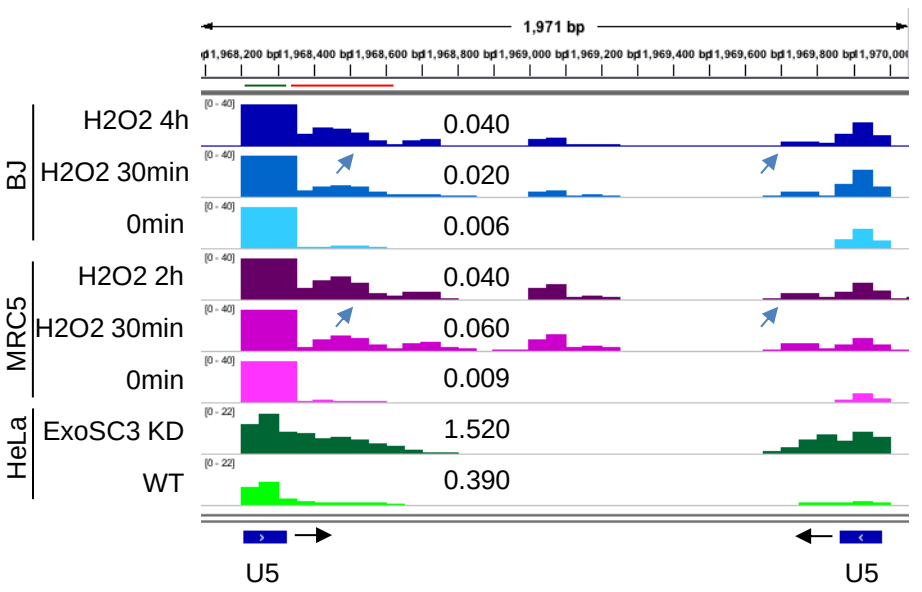

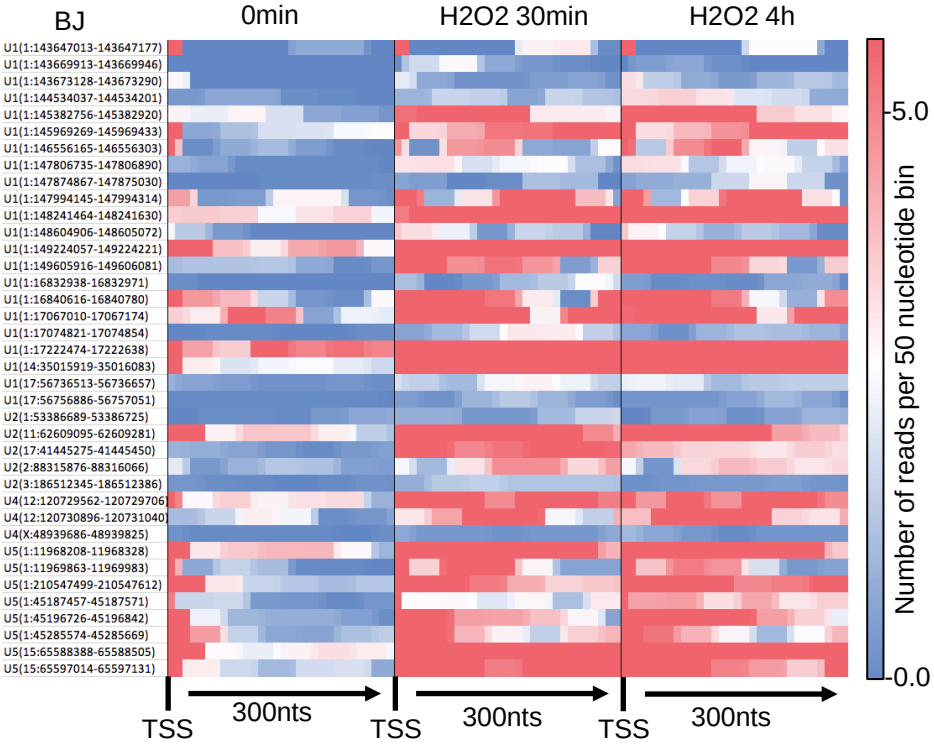

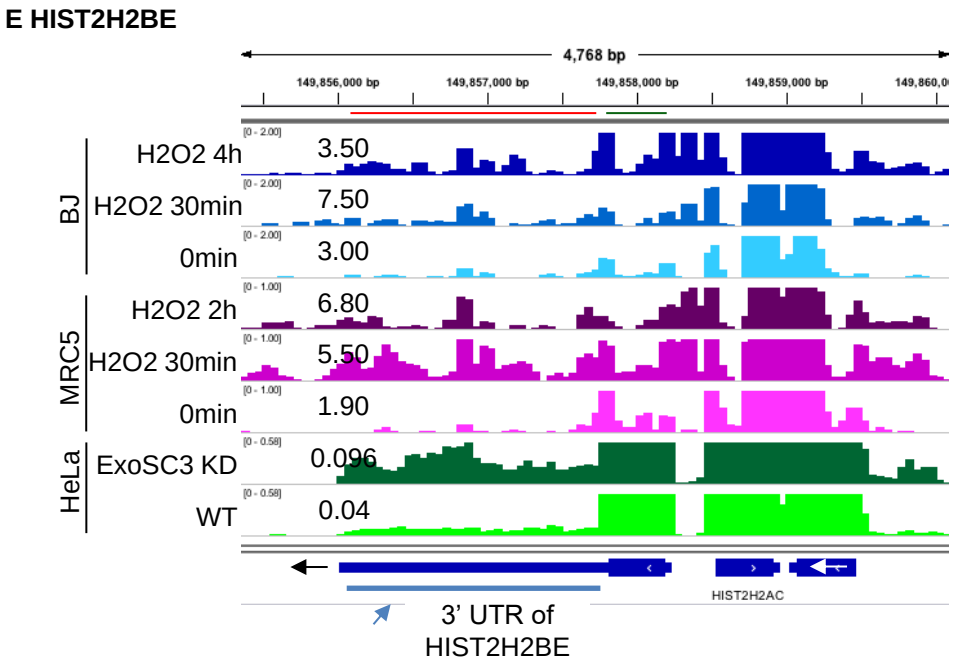

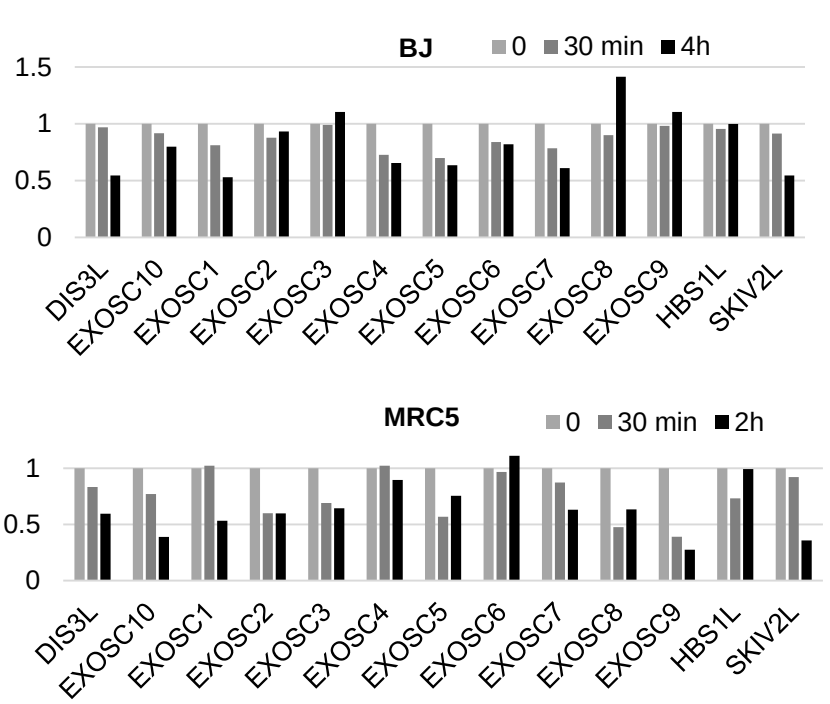

Figure 2

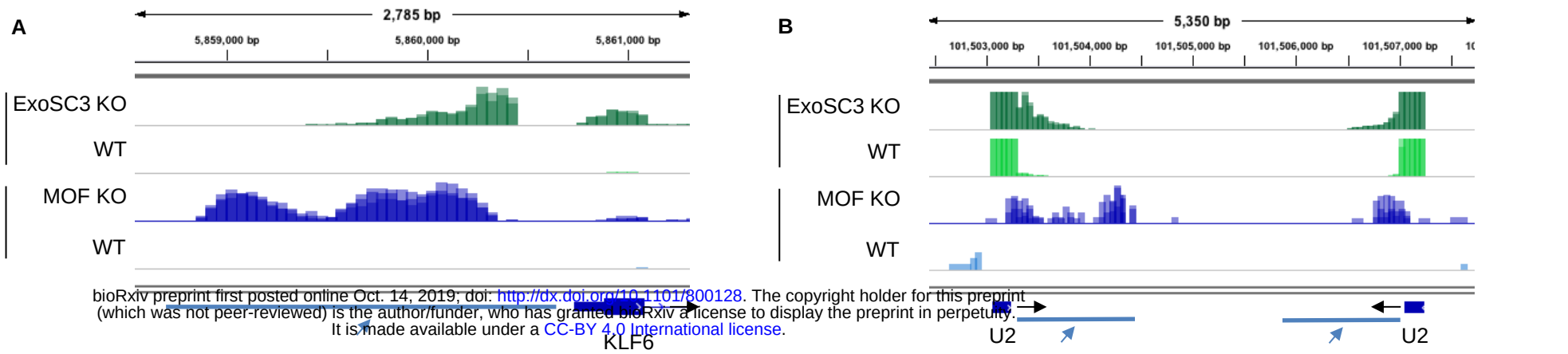

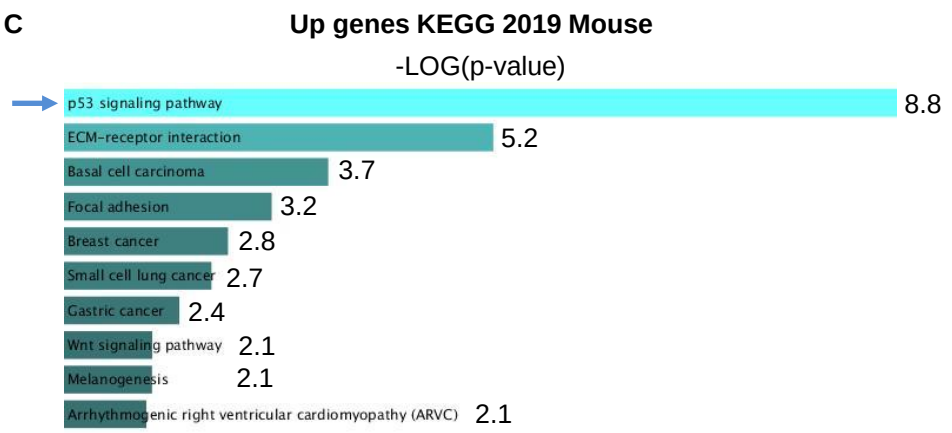

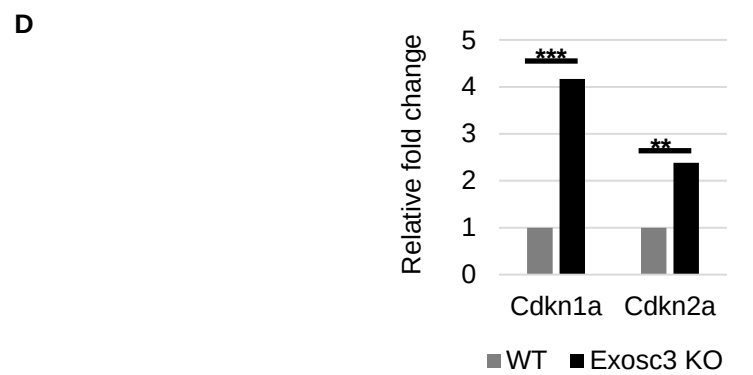

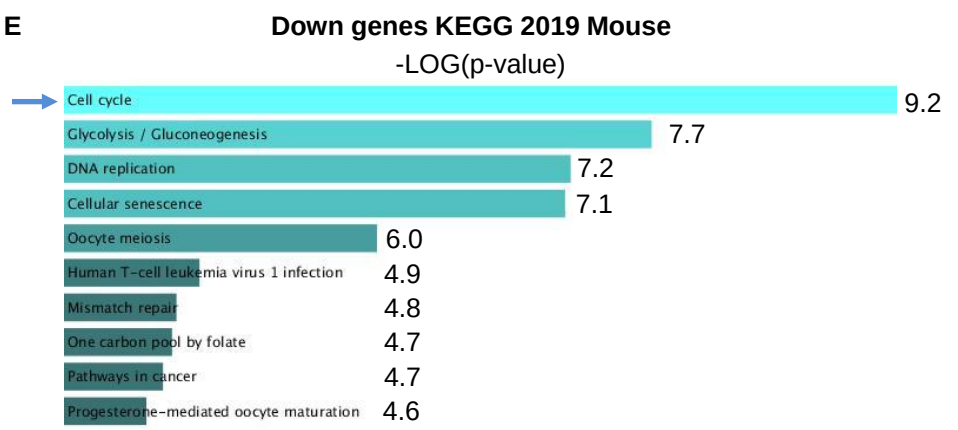

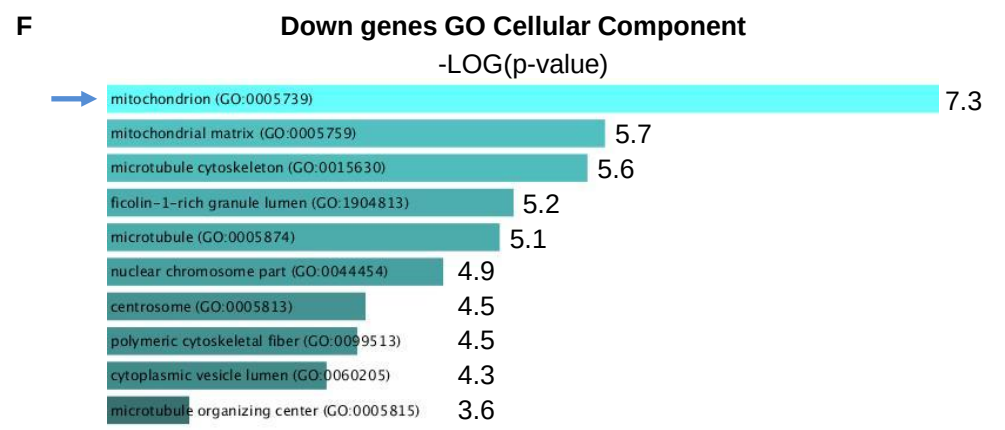

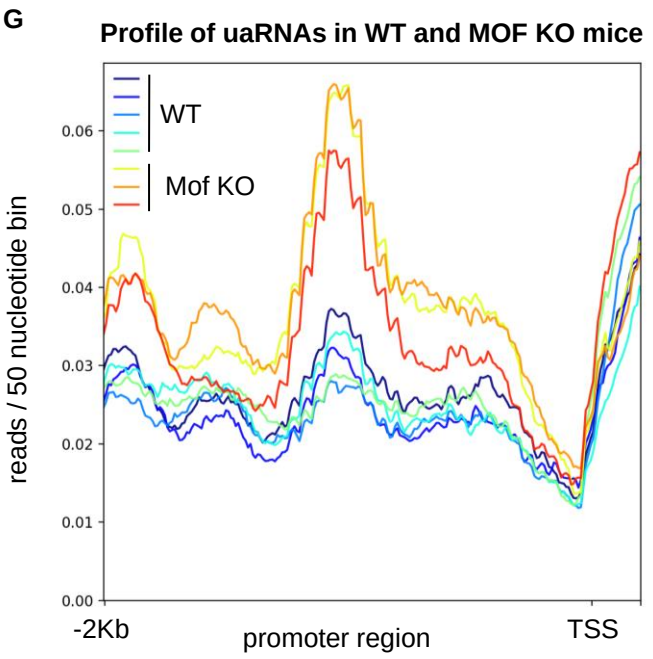

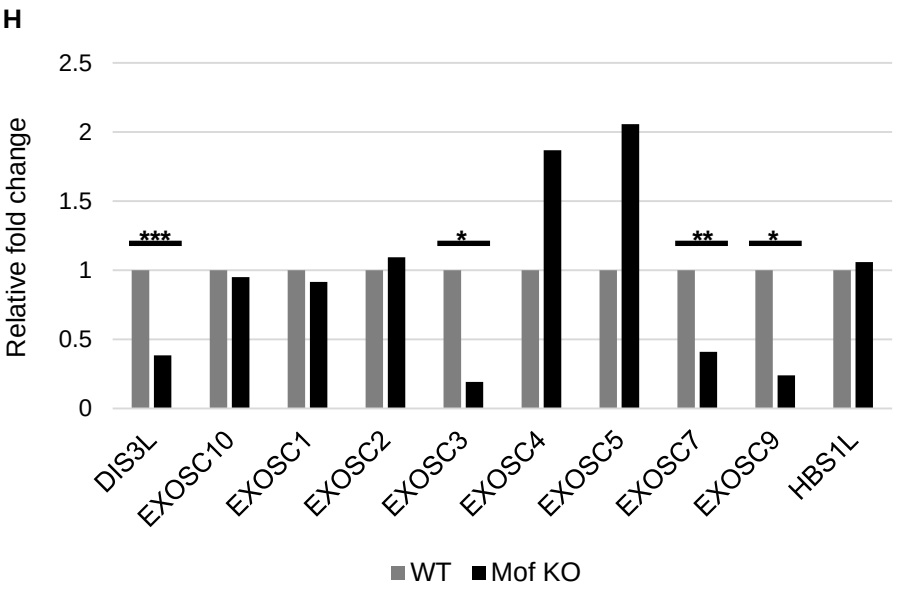

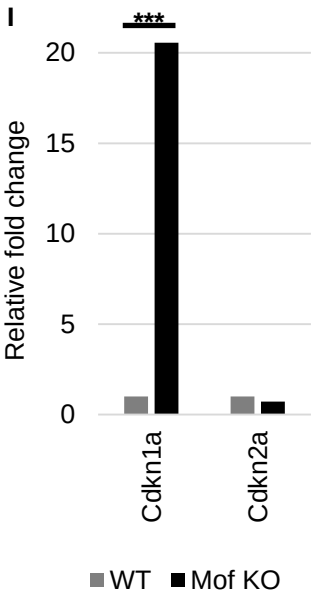

Figure 3

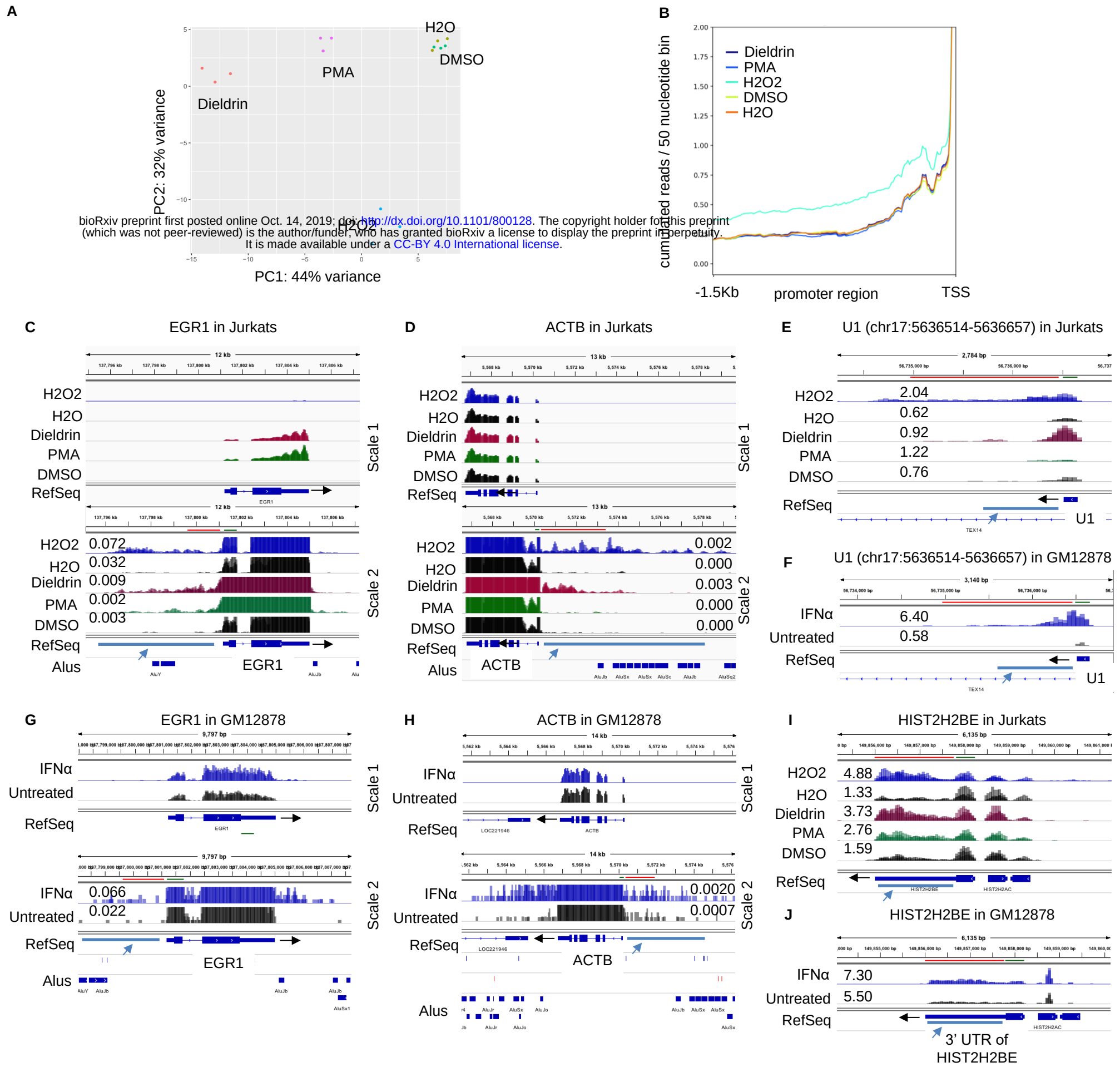

Figure 4

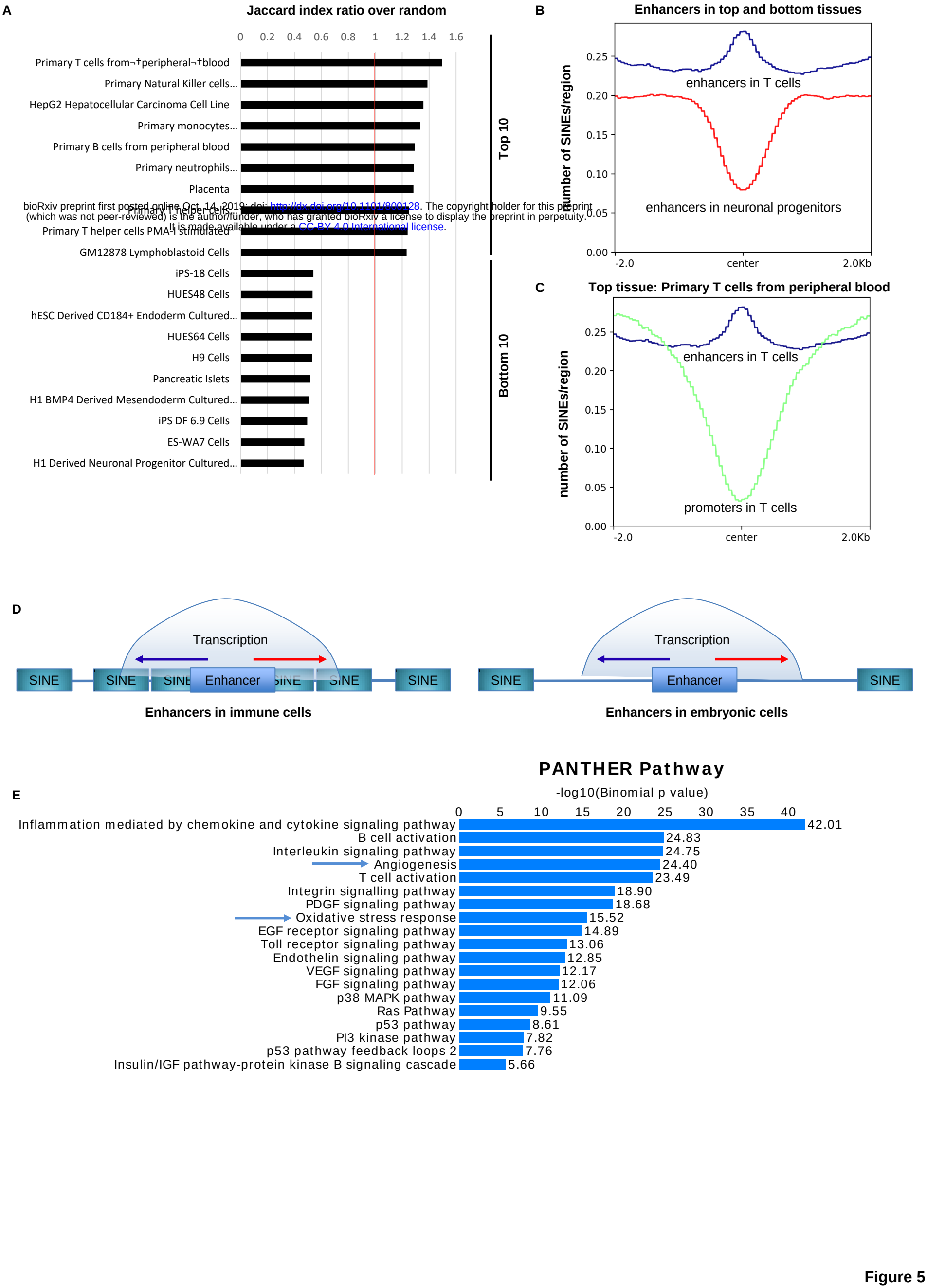

Figure 5

A FOS

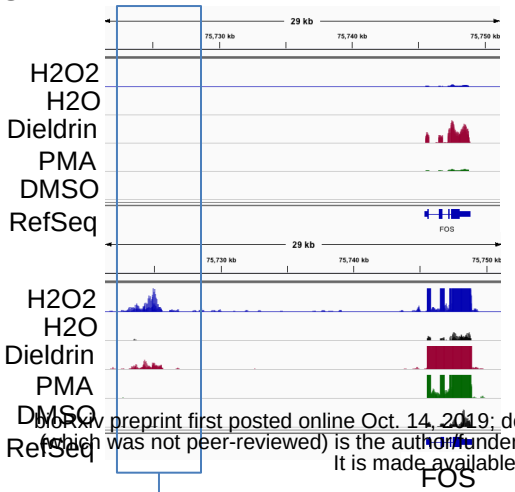

B FOS enhancer: ribodepletion *vs.* polu(A) enrichment

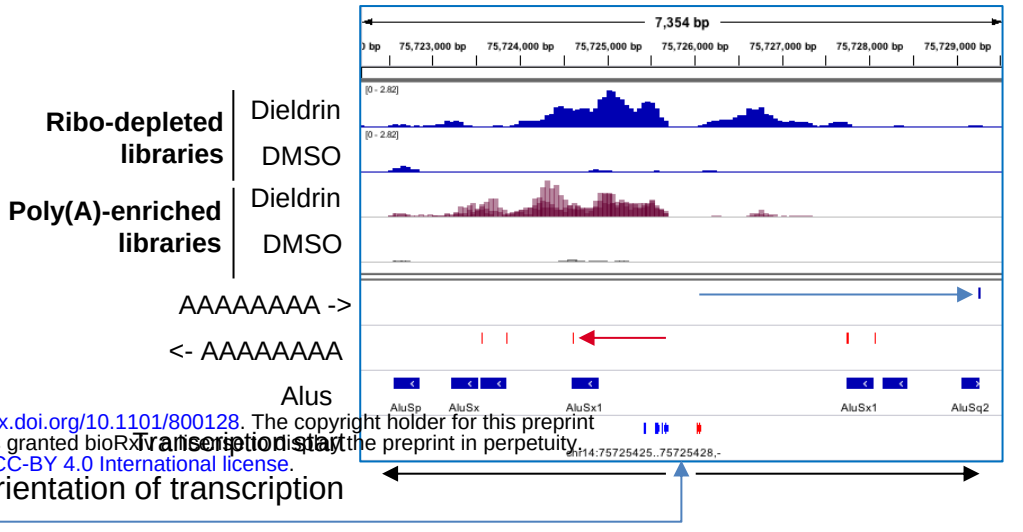

C

Bottom tissue: H1-derived neuronal progenitors

Sup. Figure 5

D Just enhancers

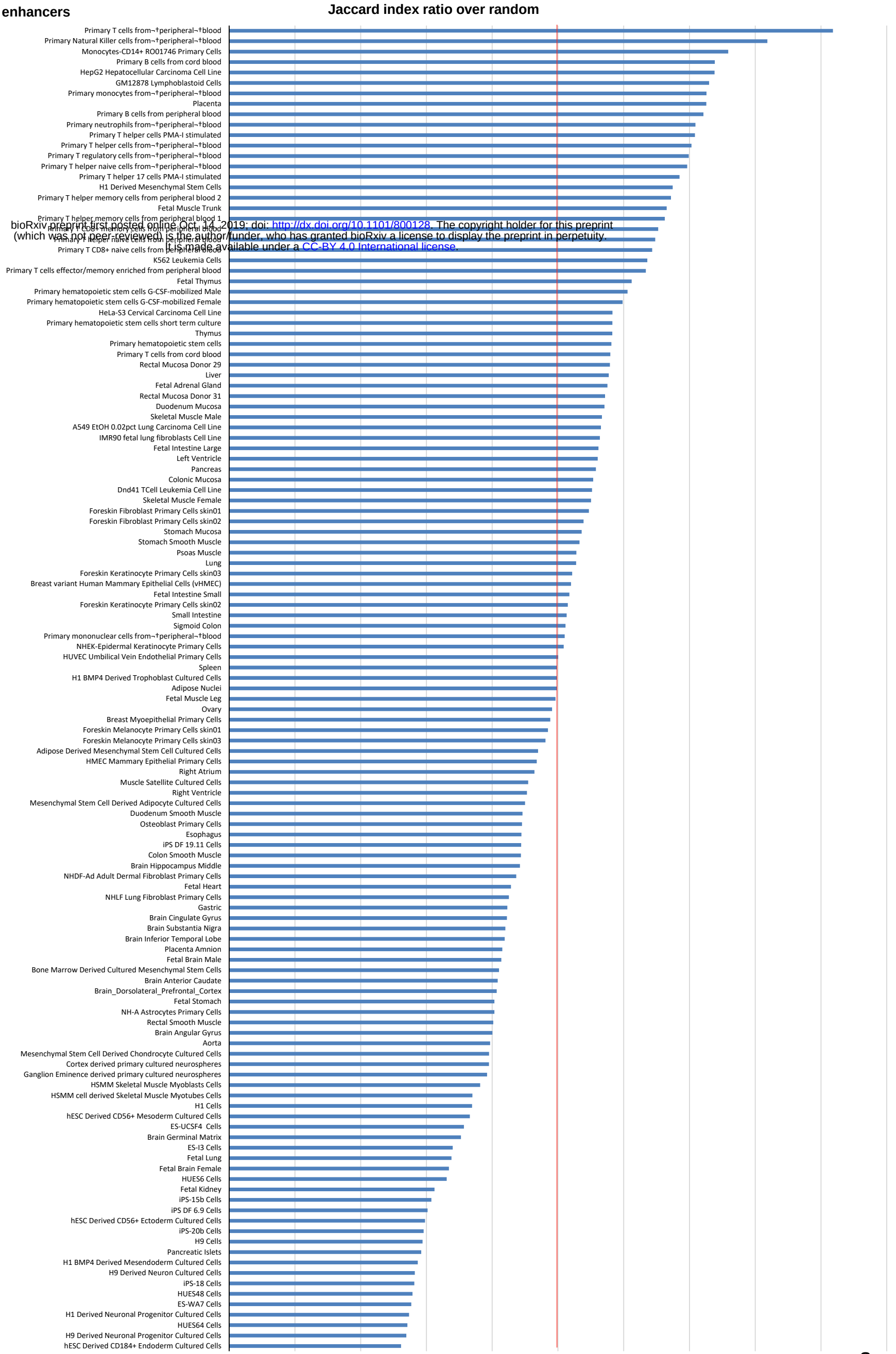

Sup. Figure 5

E

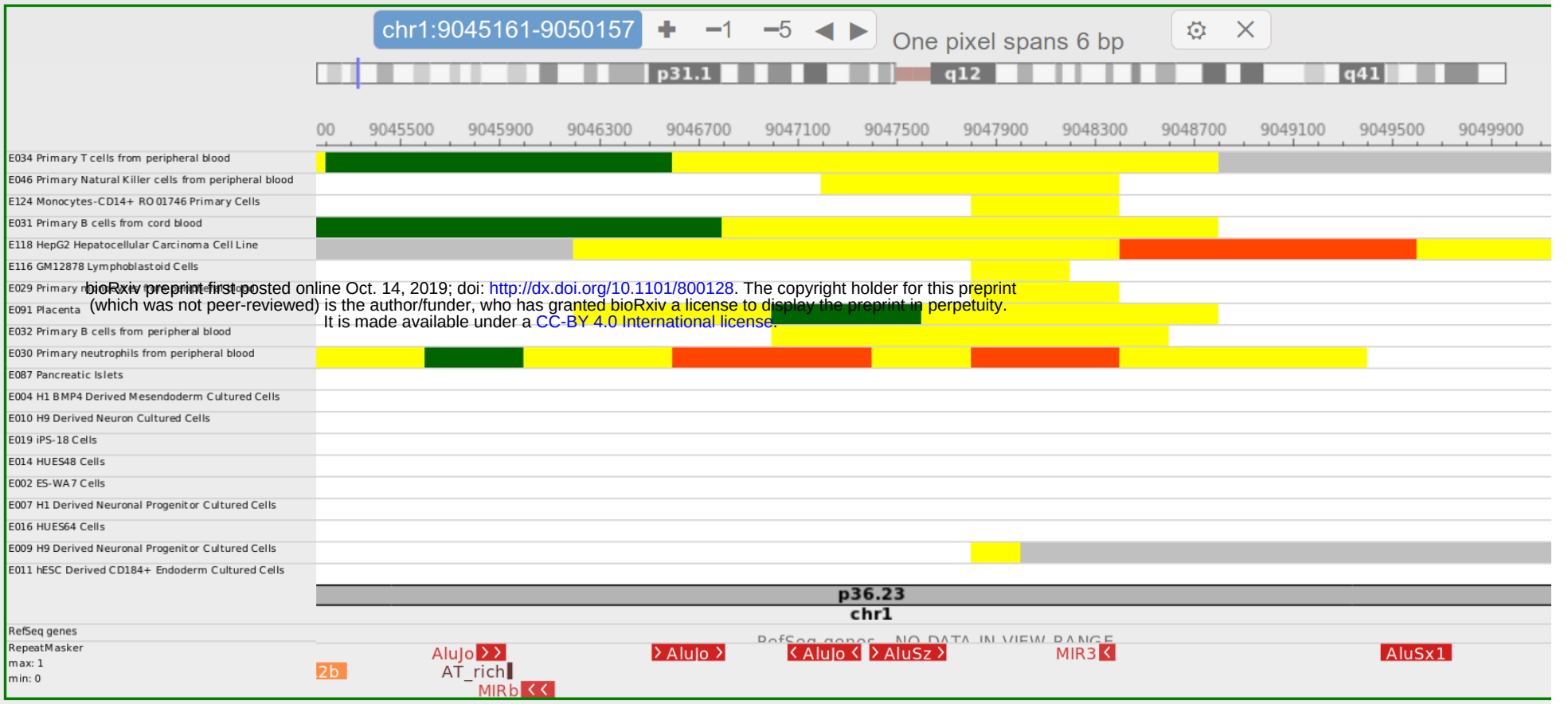

F

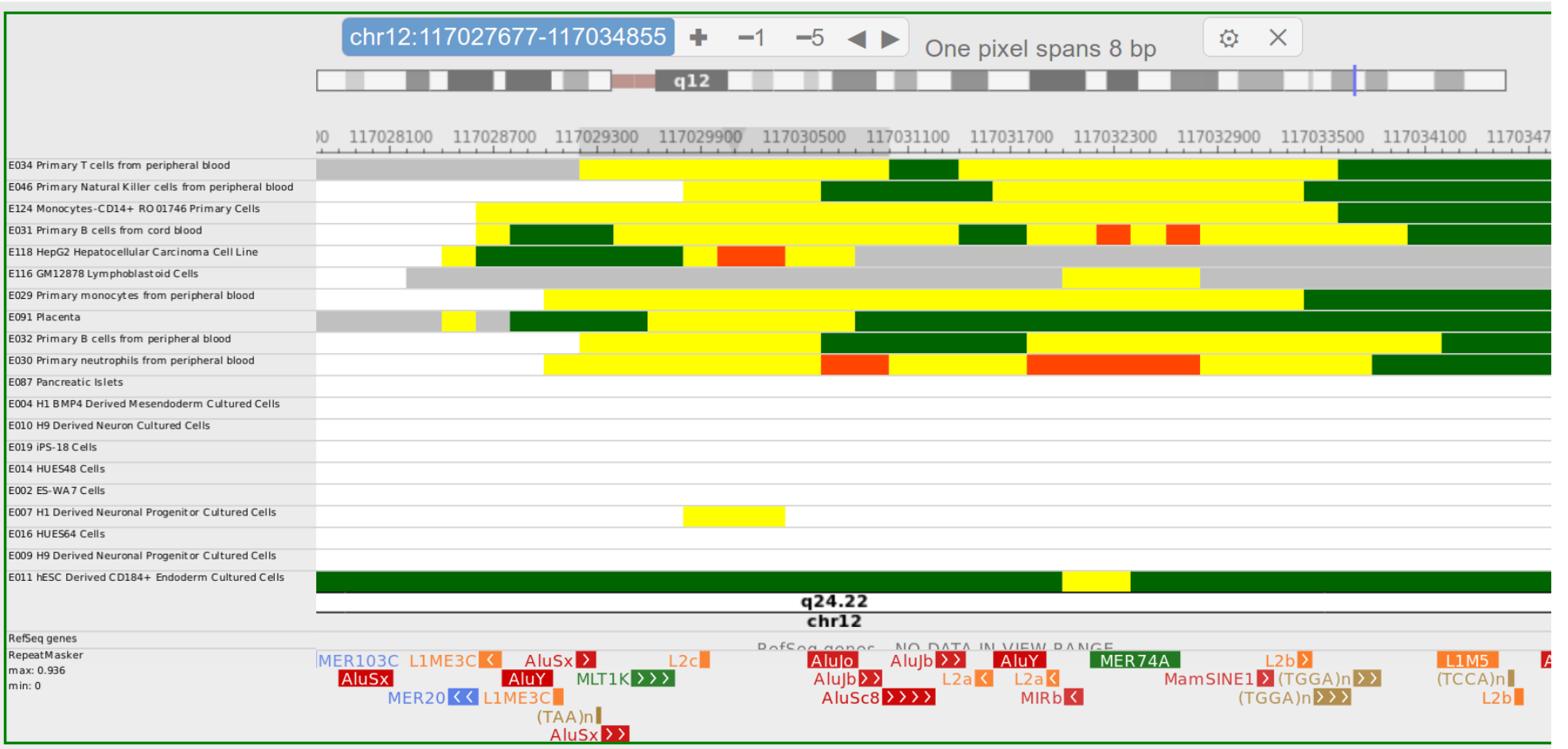

Sup. Figure 5

MODEL

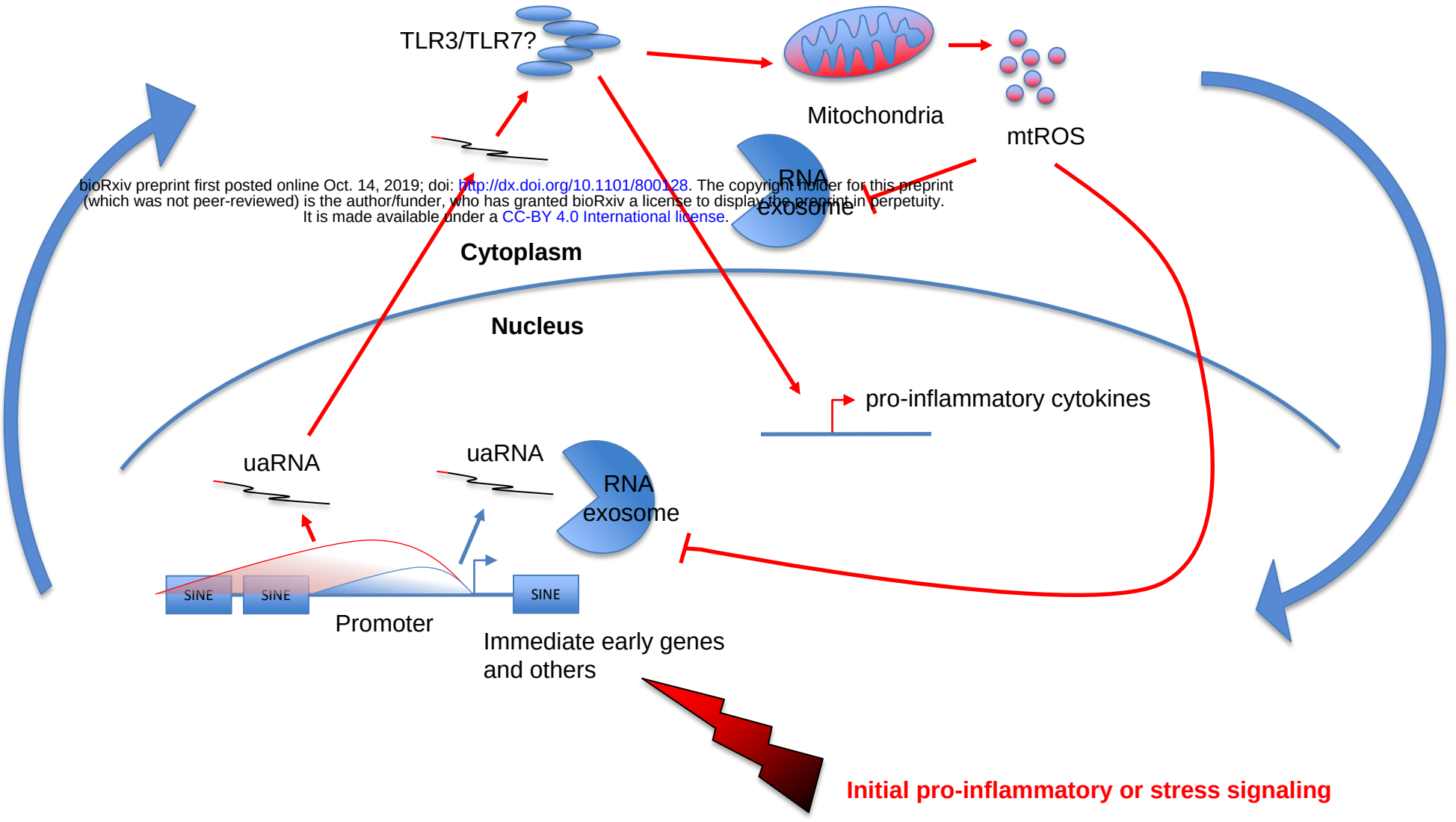

Figure 6